Supplementary Information for Surface-Attached Molecules Control *Staphylococcus aureus* Quorum Sensing and Biofilm Development

Minyoung Kevin Kim, Aishan Zhao, Ashley Wang, Zachary Z. Brown, Tom W. Muir, Howard A. Stone, and Bonnie L. Bassler

This file includes:

Supplementary Figures S1-S8

Supplementary Tables S1-S2

Supplementary Video Legends 1-3

Supplementary Note 1

Supplementary Methods

Supplementary References

Color-blind-friendly versions of Figures 1-5 and Supplementary Figures 1-8

Other supplementary information for this manuscript includes the following:

Supplementary Videos 1-3

Supplementary Figures:

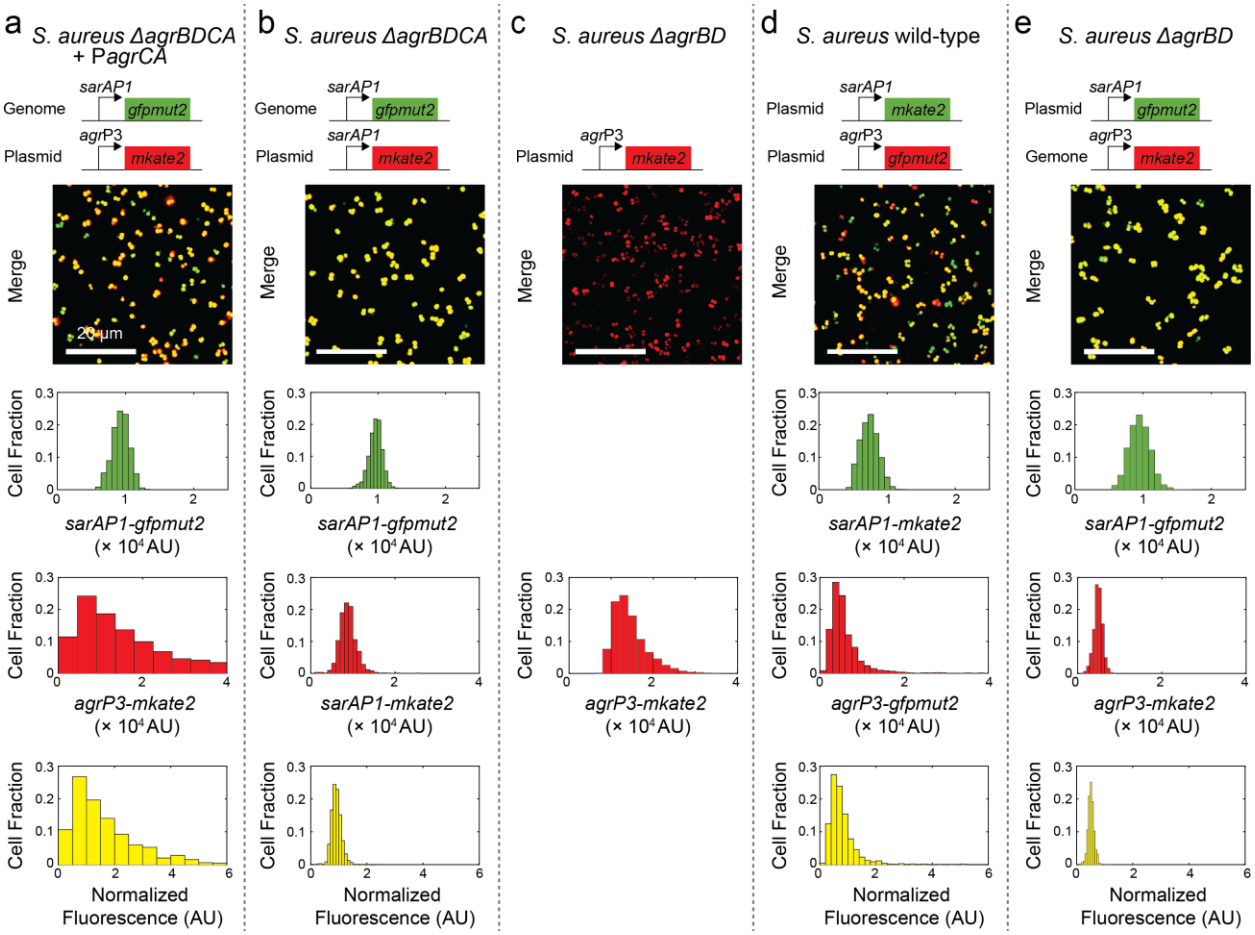

Supplementary Figure 1 | *S. aureus* exhibits heterogeneous quorum-sensing responses. a, The reporter strain is *S. aureus* Δ*agrBDCA* carrying a constitutively expressed *sarAP1-gfpmut2* transcriptional fusion in the genome. The strain also harbors the quorum-sensing-controlled *agrP3-mkate2* reporter and the *agrCA* autoinducer-detection/response genes on a plasmid under their native *agrP2* promoter. The *agrP3-mkate2* and *agrP2-agrCA* genes are cloned in the opposite orientation. **b,** The *S. aureus* Δ*agrBDCA* strain with *sarAP1-gfpmut2* in the genome and *sarAP1-mkate2* on a plasmid. **c,** The *S. aureus* Δ*agrBD* strain carrying *agrP2-agrCA* in the chromosome. The *agrP3-mkate2* fusion is carried on a plasmid. This strain does not possess the constitutive reporter gene. **d,** Wild-type *S. aureus* carrying *sarAP1-mkate2* and *agrP3-gfpmut2* on the same

plasmid. **e,** The *S. aureus* Δ*agrBD* strain carrying *agrP3-mkate2* and *agrP2-agrCA* in the chromosome. The *sarAP1-gfpmut2* fusion is carried on a plasmid. We note that in panel **d**, the fluorescent colors are reversed to make them consistent with the reporter colors shown in panel **a**. We maintained the identical color code in all panels for ease of comparison**.** The top panels show the relevant genotypes, fluorescent reporters, and an image of the fluorescent cells. Below the micrograph images, in each vertical row, are shown representative histograms of the single-cell expression from the constitutive promoter (top) and the quorum-sensing-controlled promoter (middle) from populations containing thousands of cells. Images are based on n = 3 independent experiments for each condition. The bottom panels in **a**, **d** and **e** show histograms of the normalized fluorescence (yellow), which is defined as the quorum-sensing-controlled reporter output divided by the output from the constitutive reporter in individual cells. The bottom panel in **b** shows a histogram of the normalized fluorescence (yellow), which is defined as the constitutive red fluorescent reporter output divided by the output from the constitutive green fluorescent reporter in individual cells. **a, c, e,** + 100 nM AIP-I (agonist). **b, d,** + buffer. Scale bars: 20 μm. See Supplementary Note 1 for analyses and discussion of these results.

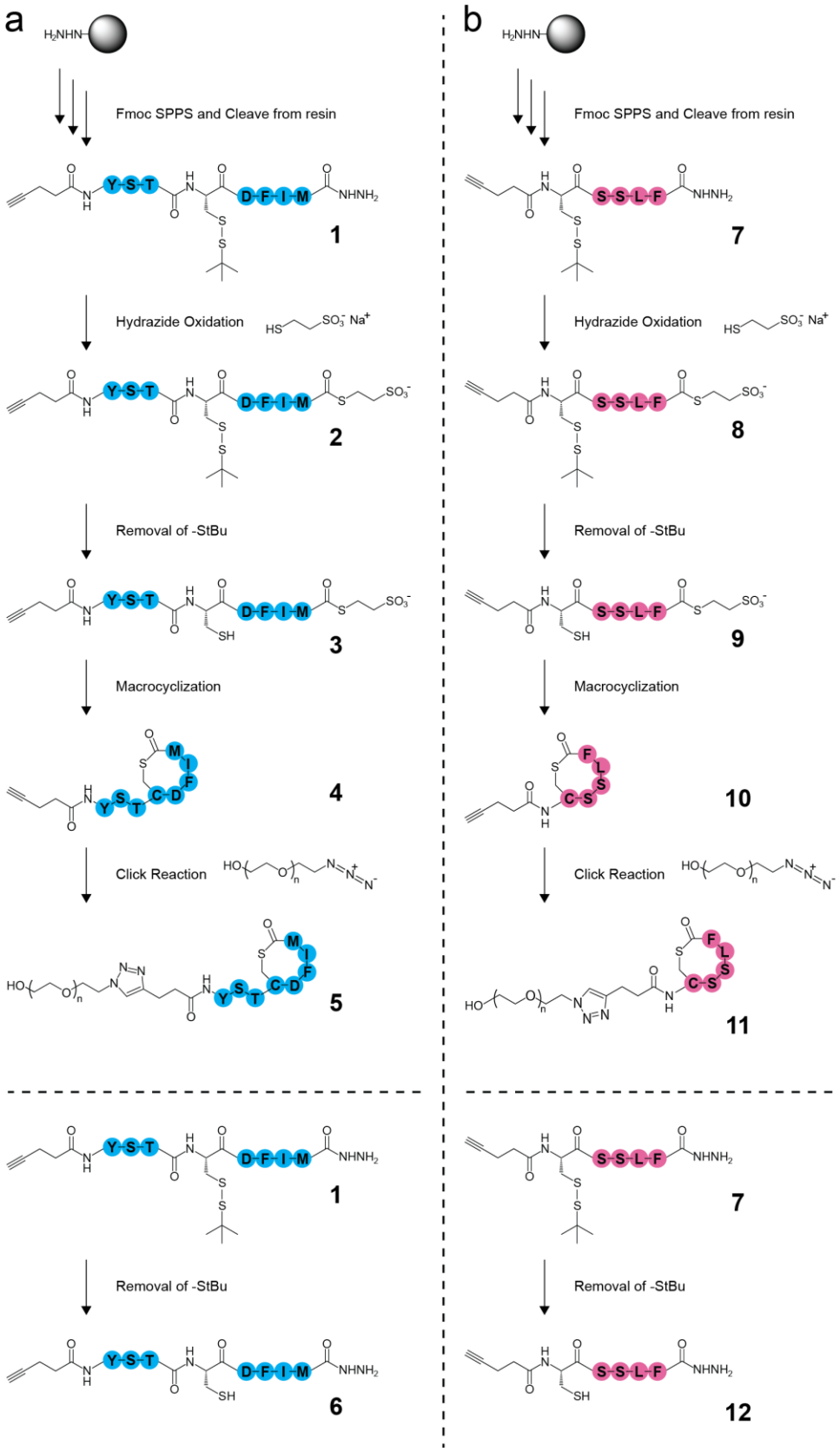
a
b
Fmoc SPPS and Cleave from resin
Hydrazide Oxidation
Removal of -StBu
Macrocyclization
Click Reaction
1
2
3
4
5
6
7
8
9
10
11
12

Supplementary Figure 2 | Synthesis scheme for a, AIP-I derivatives and b, TrAIP-II derivatives. Peptides were generated using Fmoc-based solid-phase peptide synthesis (SPPS) on hydrazine derivatized resins followed by cleavage with trifluoroacetic acid (TFA). Hydrazide peptides (**1**) and (**7**) were oxidized with $NaNO_2$ and subsequently underwent MESNa (sodium 2-sulfanylethanesulfonate) thiolysis. Thioesters (**2**) and (**8**) were purified with reverse phase-high-performance liquid chromatography (RP-HPLC), and then treated with TCEP (3,3',3"-Phosphanetriyltripropanoic acid) to remove the -StBu protecting group, and cyclized in buffer at pH = 7, generating, via intermediates (**3**) and (**9**), compounds (**4**) and (**10**), which are the Alkyne-AIP-I and Alkyne-TrAIP-II, respectively. The Alkyne-AIP-II was synthesized using the identical method. PEG_{330}-triazole-AIP-I (**5**) and PEG_{330}-triazole-TrAIP-II (**11**) were produced via the copper (I) catalyzed alkyne-azide cycloaddition (CuAAC) click reaction with O-(2-Azidoethyl) heptaethylene glycol. Alkyne-Linear-AIPs (**6**) and (**12**) were produced by removing -StBu from (**1**) and (**7**).

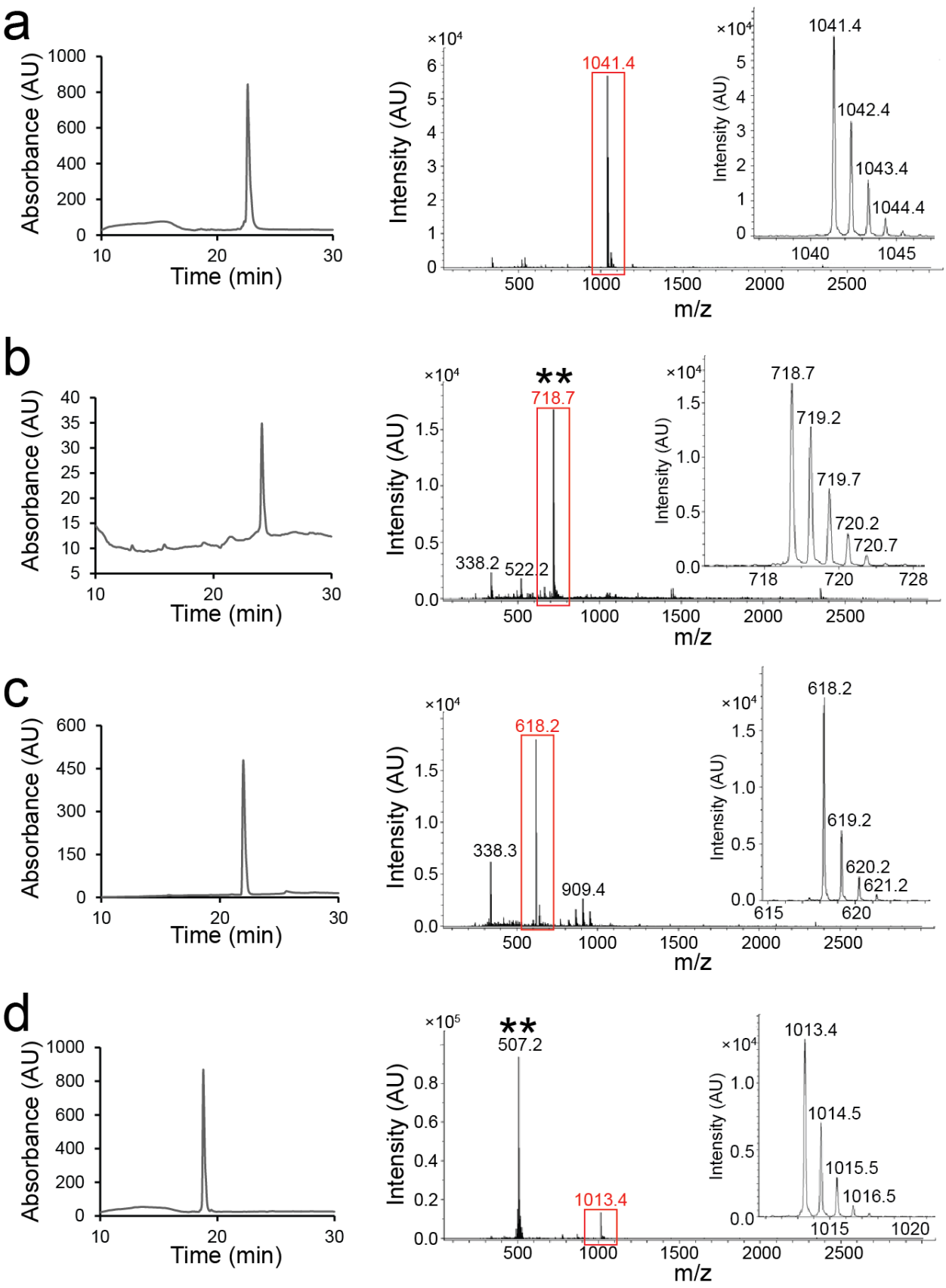
a
Absorbance (AU)
Time (min)
Intensity (AU)
m/z
1041.4
1042.4
1043.4
1044.4
b
**
718.7
719.2
719.7
720.2
720.7
338.2
522.2
c
618.2
619.2
620.2
621.2
338.3
909.4
d
507.2
1013.4
1014.5
1015.5
1016.5

Supplementary Figure 3 | Characterization of purified AIP-I and TrAIP-II derivatives by RP-HPLC (left) and electrospray ionization-mass spectrometry (ESI-MS, right). a, Alkyne-AIP-I. Expected $[M+H]^+$ = 1041.4 Da. Observed $[M+H]^+$ = 1041.4 Da. **b,** PEG_{330}-triazole-AIP-I. Expected $[M+2H]^{2+}/2$ = 718.7 Da. Observed $[M+2H]^{2+}/2$ = 718.7 Da. **c,** Alkyne-TrAIP-II. Expected $[M+H]^+$ = 618.3 Da. Observed $[M+H]^+$ = 618.2 Da. **d,** PEG_{330}-triazole-TrAIP-II. Expected $[M+H]^+$ = 1013.4 Da. Observed $[M+H]^+$ = 1013.4 Da. Red boxed peaks are magnified at the right of each panel. Double asterisks (**) denote $[M+2H]^{2+}/2$.

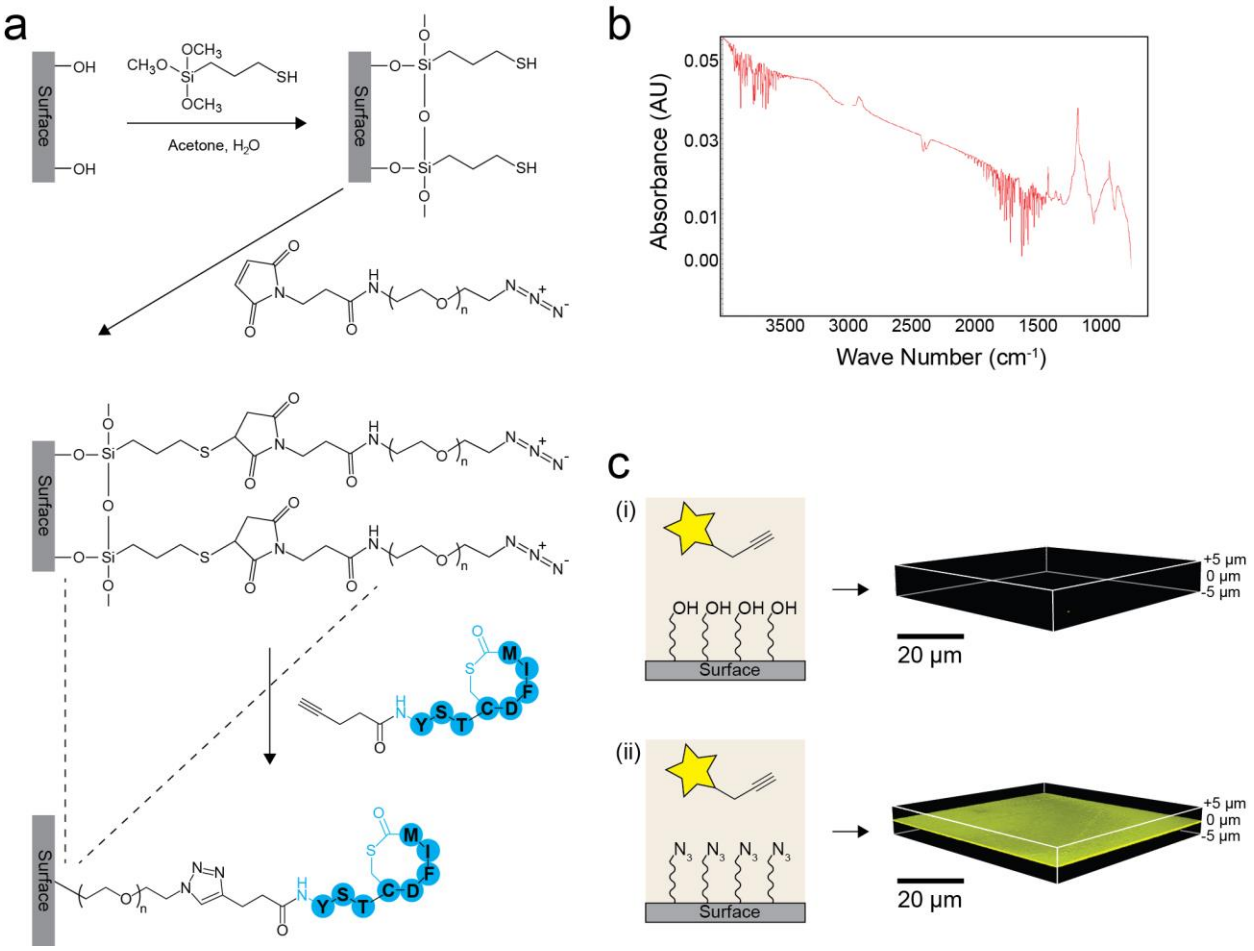

Supplementary Figure 4 | Chemical modifications of surfaces and surface chemistry characterization. a, Schematic of the reactions to generate the Surface-PEG$_{10000}$-triazole-AIP-I. The glass surface was hydroxylated using the piranha reaction, followed by silanization to attach thiol (-SH) moieties. Next, the thiol-decorated surface was linked with a PEG$_{10000}$ polymer functionalized with a maleimide moiety at one terminus, using an addition reaction. The PEG polymer linker also harbored an azide at the other terminus. This azide was subjected to a click reaction to attach molecules carrying alkyne groups, such as the Alkyne-AIP-I. **b,** Attenuated total reflectance infrared spectra of the Surface-PEG$_{10000}$-azide (See Methods for details). Peaks at 970-1250 cm^{-1} show strong signals from C-O bonds, and peaks at 2850-3000 cm^{-1} show weak signals from C-H bonds in methylene moieties. These results indicate that the PEG polymer is attached to

the surface. The azido moiety has a relatively low abundance peak due to the N_3/C-H ratio per tether being ~1/880, which is below the detection limit. The representative infrared spectra shown for the Surface-PEG_{10000}-azide was based on two independently fabricated samples, and each sample was scanned 128 times to obtain an averaged signal. **c,** The Alexa Fluor 555 dye functionalized with an alkyne moiety (Thermo Fisher, MA) was used to characterize the surfaces. (i) Surface-PEG_{10000}. (ii) Surface-PEG_{10000}-azide. Left, Schematic of the surface, which was treated with the Alexa Fluor 555 alkyne dye (depicted by yellow stars) and underwent the click reaction. Right, Three-dimensional rendering of each surface following the click reaction (51 × 51 × 10 μm^3). The results show that the Surface-PEG_{10000}-azide was successfully conjugated to the dye while the Surface-PEG_{10000} was incapable of undergoing the click reaction to attach the dye to the surface. Image (i) and (ii) are based on n = 5 and n = 8 independent experiments, respectively. Scale bars: 20 μm.

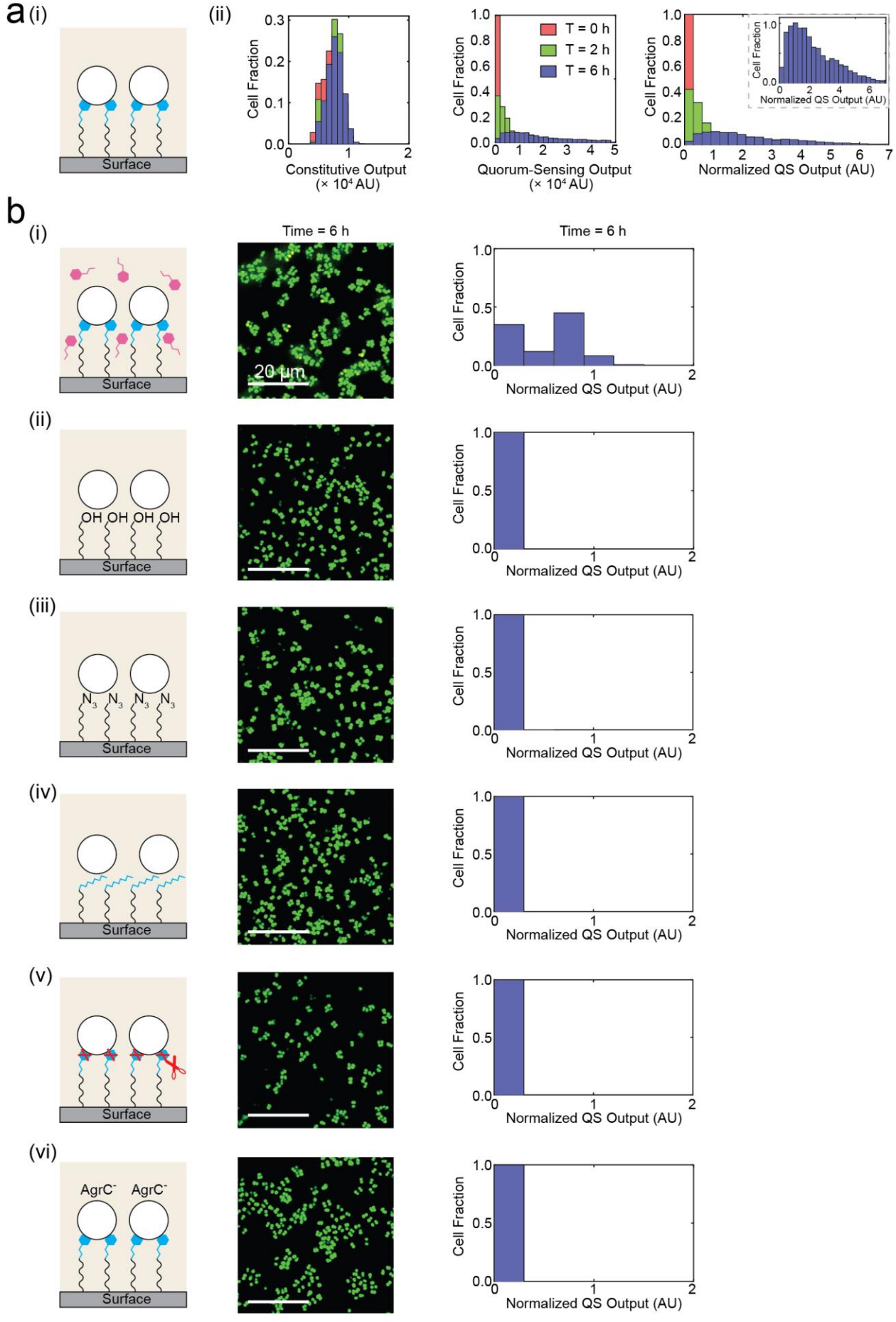
a
(i)
Surface
(ii)
Cell Fraction
Constitutive Output
(× 10⁴ AU)
T = 0 h
T = 2 h
T = 6 h
Quorum-Sensing Output
(× 10⁴ AU)
Normalized QS Output (AU)
b
(i)
Time = 6 h
20 μm
(ii)
OH OH OH OH
(iii)
N3 N3 N3 N3
(iv)
(v)
(vi)
AgrC⁻ AgrC⁻

Supplementary Figure 5 | *S. aureus* Agr quorum sensing is activated by surface-attached AIP-I. a, (i) Schematic of the experimental strategy showing the Surface-PEG_{10000}-triazole-AIP-I and the addition of *S. aureus* cells (depicted as white circles) in liquid. (ii) Distribution of constitutive output (left), quorum-sensing-controlled output (middle), and the normalized quorum-sensing-controlled output (right) from single-cell analyses at T = 0, 2, 6 h. The magnified graph in the inset shows the normalized quorum-sensing output at T = 6 h taken from the left panel and plotted for the range of 0 to 0.1. **b,** Schematics (left), merged images at T = 6 h (middle), and normalized quorum-sensing outputs at T = 6 h from single-cell analyses (right) of control experiments characterizing the different surface chemistries from Fig. 2c of the main text. (i) Surface-PEG_{10000}-triazole-AIP-I + 2.5 μM TrAIP-II in solution, (ii) Surface-PEG_{10000}, which were exposed to the click solution containing the Alkyne-AIP-I for 3 h and rinsed with 50 % dimethyl sulfoxide in water. (iii) Surface-PEG_{10000}-azide, and (iv) Surface-PEG_{10000}-triazole-Linear-AIP-I were generated via the click reaction between the Surface--PEG_{10000}-azide and compound **6** in Fig. S2a. (v) Surface-PEG_{10000}-triazole-AIP-I was produced as described and, subsequently, the thioester ring was opened by treatment with 10 mM cysteine (depicted as red scissors in the schematic) in 100 mM phosphate buffer (pH = 7) for 1 h. (vi) Surface-PEG_{10000}-triazole-AIP-I was seeded with *S. aureus* cells that lack the AgrC receptor (the designation $AgrC^-$ is shown above the white circles depicting the cells). The strain is called MK245. All images shown in Fig. S5 are based on n = 3 independent experiments for each condition; one representative image for each condition was chosen from ~ 50 images acquired from different regions of each surface. Scale bars: 20 μm. All histograms shown in Fig. S5 are representatives from a single experiment examining bacterial populations containing thousands of cells. Three independent experiments were performed. All experiments yielded similar results.

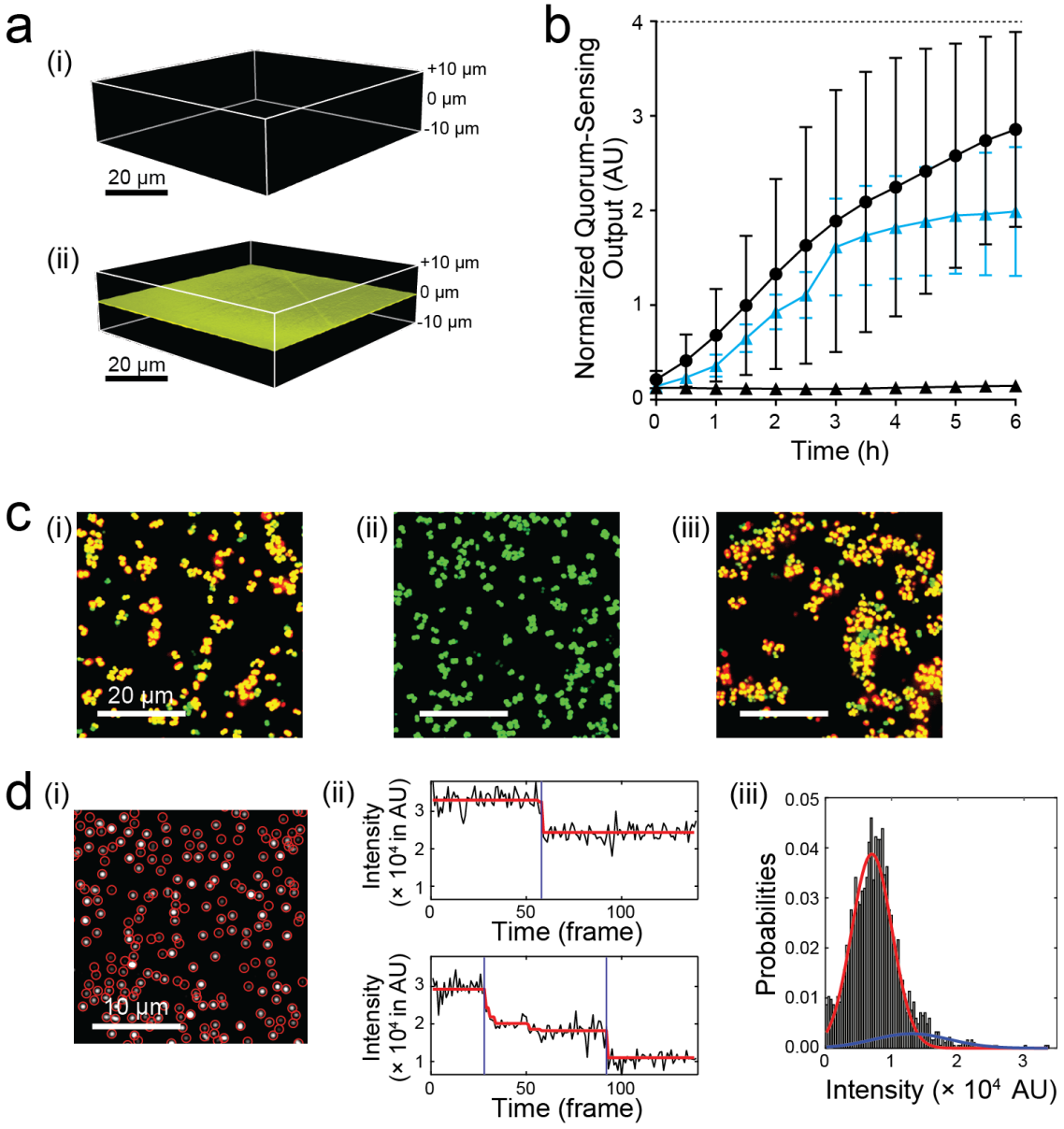
a
(i)
+10 μm
0 μm
-10 μm
20 μm
(ii)
+10 μm
0 μm
-10 μm
20 μm
b
Normalized Quorum-Sensing Output (AU)
Time (h)
c
(i)
20 μm
(ii)
(iii)
d
(i)
10 μm
(ii)
Intensity (× 10⁴ in AU)
Time (frame)
Intensity (× 10⁴ in AU)
Time (frame)
(iii)
Probabilities
Intensity (× 10⁴ AU)
e
AIP-I/(AIP-I + Linear-AIP-I) (%)
Normalized Quorum-Sensing Output (AU)
Coverage Density of Surface-AIP-I (× 10⁴ μm⁻²)

Supplementary Figure 6 | The requirements for Agr quorum-sensing activation by surface-attached AIP-I. a, Alexa Fluor 555 alkyne dye (Thermo Fisher, MA) was used to detect azide functional groups on coated surfaces. Three-dimensional rendering of each surface following the click reaction ($51 \times 51 \times 10$ μm^3). (i) Surface-PEG_{400} and (ii) Surface-PEG_{400}-azide. Images are based on n = 3 independent experiments. Only the Surface-PEG_{400}-azide successfully underwent the click reaction to generate the Surface-PEG_{400}-triazole-dye. **b,** The *S. aureus* Agr quorum-sensing output in response to the Surface-PEG_{10000}-triazole-AIP-I (black circles), Surface-PEG_{400}-triazole-AIP-I (black triangles), and Surface-PEG_{400}-triazole-AIP-I + 50 nM AIP-I in solution (blue triangles). Data points indicate means and error bars denote standard deviations from triplicate experiments. **c,** Merged images at T = 6 h. (i) Surface-PEG_{10000}-triazole-AIP-I. (ii) Surface-PEG_{400}-triazole-AIP-I. (iii) Surface-PEG_{400}-triazole-AIP-I + 50 nM AIP-I in solution. Images are based on n = 3 independent experiments for each condition; one representative image for each condition was chosen from ~ 50 images acquired from different regions of each surface. Scale bars: 20 μm. **d,** Single-molecule analysis to quantify surface coverage density. (i) A representative image is shown of individually discernable fluorescent spots on the surface, which were photobleached. Images are based on n = 3 independent experiments. The Surface-PEG_{10000}-azide had reacted with 0.1 – 10 nM Alexa Fluor 555 alkyne fluorophore. Using a peak-finding algorithm, background-subtracted intensities of each spot were measured over time (red circles in the image). Scale bar: 10 μm. (ii) Two representative time courses of fluorescence emission for a fluorophore-labeled spot, displaying stepwise decreases in intensity. Most spots decreased in intensity in one step following bleaching (top), and a small number of spots bleached in two steps (bottom). (iii) Fitting the bleaching step sizes for over 3,600 spots with a normal distribution, provided the average single-molecule intensity (7,000 (AU)). This value was used to quantify

surface coverage density of the Surface-PEG_{10000}-azide that had reacted with 100 μM Alexa Fluor 555 alkyne fluorophore (a typical click reaction concentration used in this study). The distribution was based on cumulative data from 5 independent experiments assessing dye-linked surfaces. **e,** The coverage density of surface-attached AIP-I affects the *S. aureus* Agr quorum-sensing output. The surface coverage density of active AIP-I was reduced by mixing Alkyne-AIP-I and Alkyne-Linear-AIP-I at different ratios prior to attachment to the surface while maintaining the total concentration of substrate for attachment constant at 100 μM. The zero-coverage density of surface-attached AIP-I denotes the surface containing only the Linear-AIP-I. The normalized Agr quorum-sensing outputs were measured 3 h after the *S. aureus* reporter strain was introduced onto the surfaces with different coverage densities. Data points indicate means and error bars denote upper and lower limits from two independent experiments.

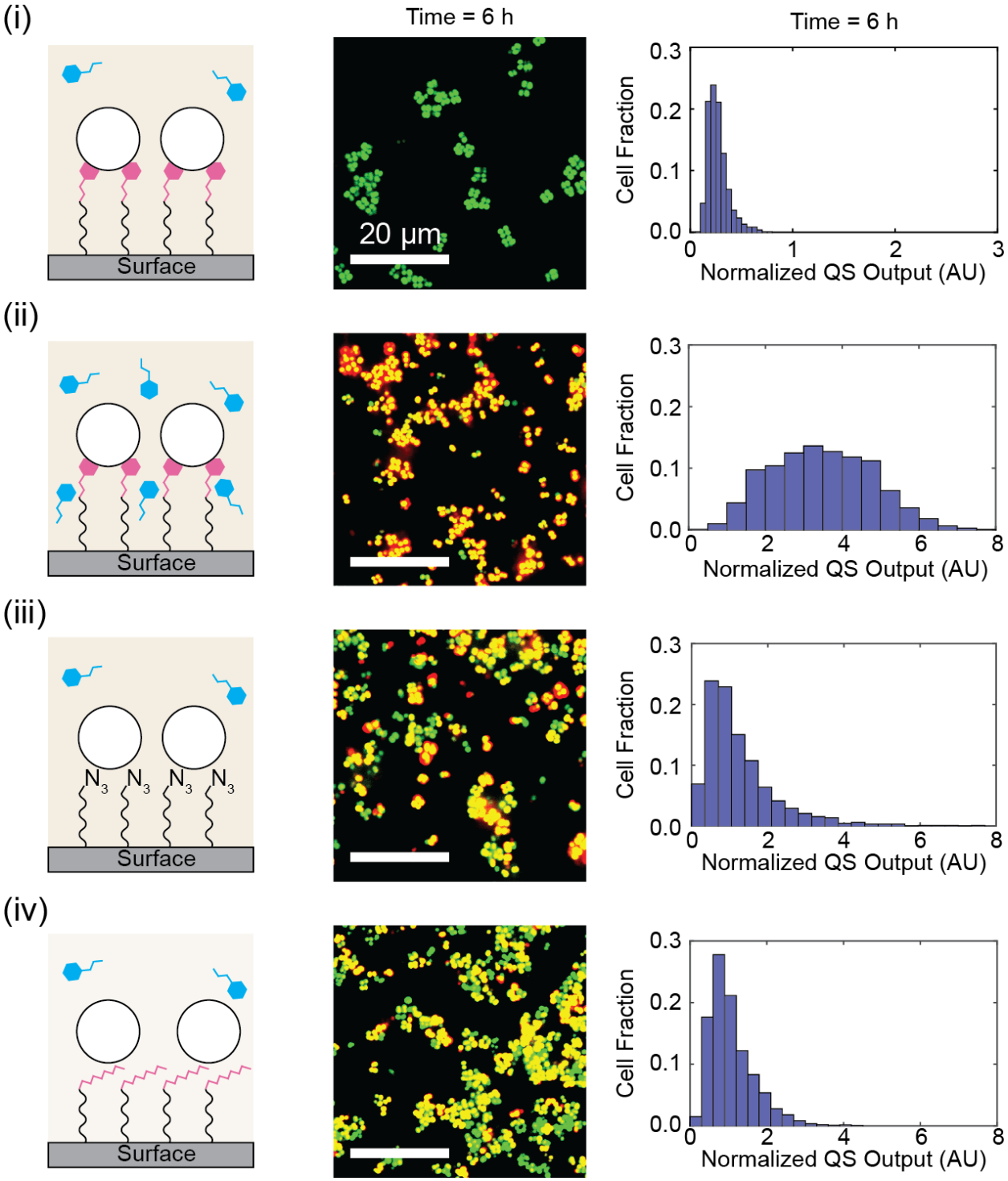

Supplementary Figure 7 | *S. aureus* Agr quorum sensing is inhibited by surface-attached TrAIP-II. (i-iv) Schematics (left), merged images at T = 6 h (middle), and normalized quorum-sensing outputs at T = 6 h from single-cell analyses (right). (i) Surface-PEG_{10000}-triazole-TrAIP-

II + 30 nM AIP-I in solution, (ii) Surface-PEG_{10000}-triazole-TrAIP-II + 1 μM AIP-I in solution, (iii) Surface-PEG_{10000}-azide + 30 nM AIP-I in solution, and (iv) Surface-PEG_{10000}-triazole-Linear-TrAIP-II + 30 nM AIP-I in solution. Surface-PEG_{10000}-triazole-Linear-TrAIP-II was produced via the click reaction between the Surface--PEG_{10000}-azide and compound **12** in Fig. S2b. Images are based on n = 3 independent experiments for each condition; one representative image for each condition was chosen from ~ 50 images acquired from different regions of each surface. Scale bars: 20 μm. All histograms shown in Fig. S7 are representatives from a single experiment examining bacterial populations containing thousands of cells. Three independent experiments were performed. All experiments yielded similar results.

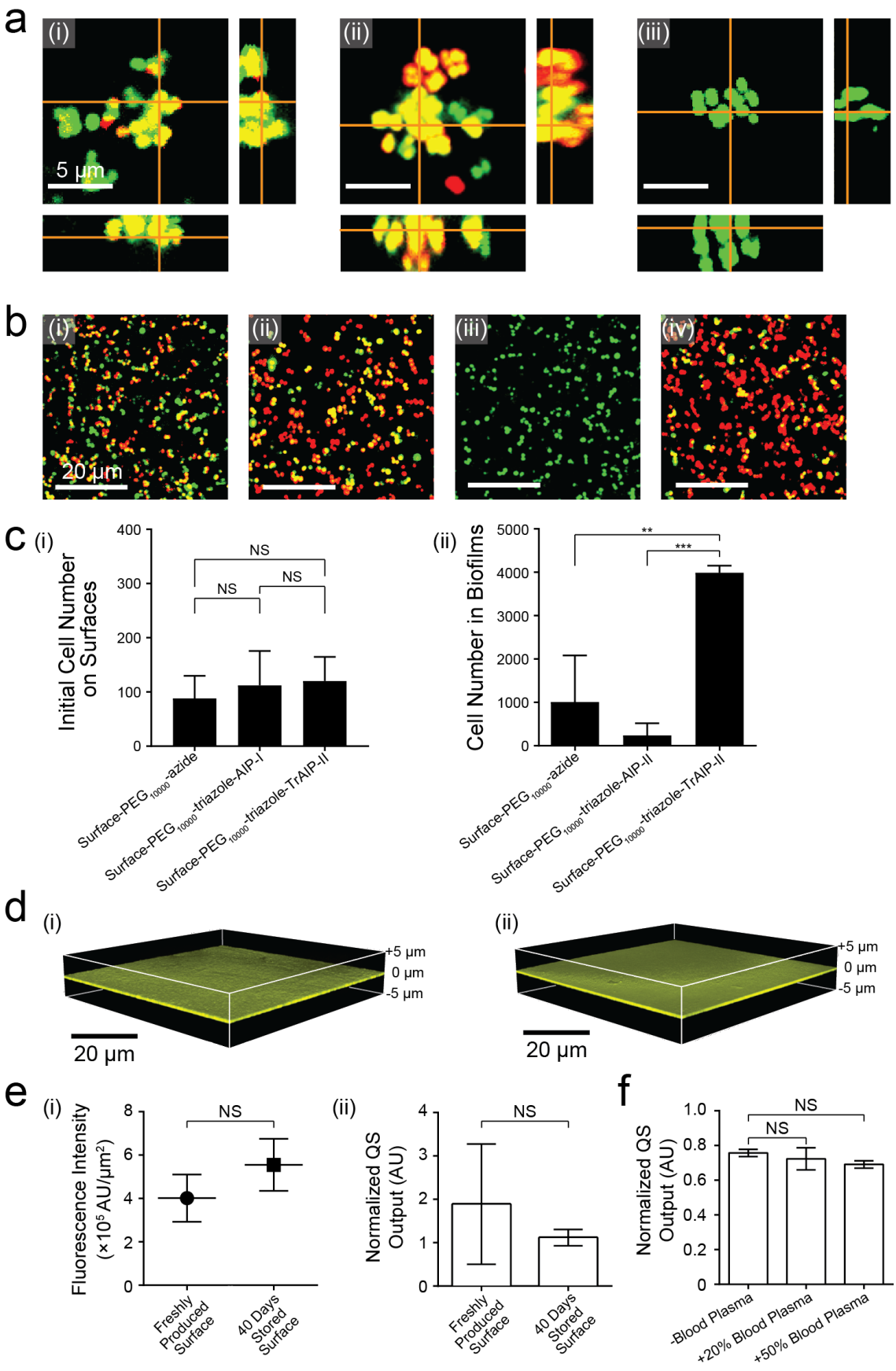
a
(i)
(ii)
(iii)
5 μm
b
(i)
(ii)
(iii)
(iv)
20 μm
c
(i)
Initial Cell Number on Surfaces
400
300
200
100
0
NS
NS
NS
Surface-PEG10000-azide
Surface-PEG10000-triazole-AIP-I
Surface-PEG10000-triazole-TrAIP-II
(ii)
Cell Number in Biofilms
5000
4000
3000
2000
1000
0
**
***
Surface-PEG10000-azide
Surface-PEG10000-triazole-AIP-II
Surface-PEG10000-triazole-TrAIP-II
d
(i)
+5 μm
0 μm
-5 μm
20 μm
(ii)
+5 μm
0 μm
-5 μm
20 μm
e
(i)
Fluorescence Intensity (×10⁵ AU/μm²)
8
6
4
2
0
NS
Freshly Produced Surface
40 Days Stored Surface
(ii)
Normalized QS Output (AU)
4
3
2
1
0
NS
Freshly Produced Surface
40 Days Stored Surface
f
Normalized QS Output (AU)
1.0
0.8
0.6
0.4
0.2
0
NS
NS
-Blood Plasma
+20% Blood Plasma
+50% Blood Plasma

Supplementary Figure 8 | Quorum-sensing response of wild-type *S. aureus* to surface-attached AIP-I, AIP-II, and TrAIP-II, chemical modification of metal and plastic surfaces, and examination of stability of the chemically-modified surfaces. a, Centered merged images showing single optical sections of the x-y plane at 2 μm above the interface of the surface and the cell cluster, with z projections shown to the right (x-z plane) and below (y-z plane). Wild-type *S. aureus agr-I* (RN6390b) was grown for 3 h after inoculation on (i) Surface-PEG_{10000}-azide, (ii) Surface-PEG_{10000}-triazole-AIP-I, and (iii) Surface-PEG_{10000}-triazole-TrAIP-II. Note: The fluorescent colors for wild-type *S. aureus agr-I* (RN6390b) are reversed to make them consistent with the colors of the reporter strains in the main text; green: constitutive fluorescence, red: quorum-sensing-controlled fluorescence. Images are based on n = 3 independent experiments for each condition; one representative image for each condition was chosen from ~ 50 images acquired from different regions of each surface. **b,** Merged fluorescent images of *S. aureus* MRSA *agr-I* cells grown on the modified surfaces at T = 6 h. Note: The fluorescent colors for the *S. aureus* MRSA cells are reversed to make them consistent with the colors of the reporter strains in the main text; green: constitutive fluorescence, red: quorum-sensing-controlled fluorescence. (i) Surface-PEG_{10000}-azide, (ii) Surface-PEG_{10000}-triazole-AIP-I, (iii) Surface-PEG_{10000}-triazole-TrAIP-II, and (iv) Surface-PEG_{10000}-triazole-TrAIP-II + 1 μM AIP-I in bulk. Images are based on n = 2 independent experiments for each condition; one representative image for each condition was chosen from ~ 50 images acquired from different regions of each surface. Scale bars: 20 μm. **c,** (i) The initial number of *S. aureus agr-I* cells (strain RN6390b) on the designated modified surfaces (225 × 225 μm^2). Data points indicate means and error bars denote standard deviations from triplicate experiments. NS indicates no significant difference for an ANOVA test with Tukey-Kramer post hoc analysis for pairwise comparisons. (ii) Number of *S. aureus agr-II* cells (strain

RN6607) in biofilms grown for 18 h on the designated modified surfaces (225 × 225 × 44 μm^3). Data points indicate means and error bars denote standard deviations from triplicate experiments. ** = P < 0.005 and *** = P < 0.0005 for an ANOVA test with Tukey-Kramer post hoc analysis for pairwise comparisons. **d,** The Alexa Fluor 555 dye functionalized with an alkyne moiety (Thermo Fisher, MA) was used to characterize coating of gold and PDMS surfaces. Three-dimensional rendering of each surface following the click reaction (51 × 51 × 10 μm^3). (i) Gold-based Surface-PEG_{5000}-triazole-dye. (ii) PDMS-based Surface-PEG_{10000}-triazole-dye. Images in panels (i) and (ii) are based on n = 2 independent experiments. Chemical modifications of gold- and PDMS-coated surfaces are described in the Methods section. The results show that both metal and plastic coated surfaces were successfully conjugated to the dye using the click reaction. Scale bars: 20 μm. **e,** Investigation of stability of coated surfaces. (i) Mean surface fluorescence intensities were measured from freshly-prepared Surface-PEG_{10000}-triazole-dye (circle) and the Surface-PEG_{10000}-triazole-dye following 40 days of storage (square). Data points indicate means and error bars denote standard deviations from triplicate experiments. (ii) The normalized Agr quorum-sensing output was measured 3 h after the *S. aureus agr-I* reporter strain was introduced onto a freshly-prepared Surface-PEG_{10000}-triazole-AIP-I (left) and onto an identical surface following 40 days of storage (right). Data points indicate means and error bars denote standard deviations from triplicate experiments. NS indicates no significant difference with two-tailed t-tests for pairwise comparisons. **f,** The normalized Agr quorum-sensing output was measured 3 h after the *S. aureus agr-I* reporter strain was introduced onto the Surface-PEG_{10000}-triazole-AIP-I that was never exposed to blood plasma (left) or that had been pre-treated with 100% human blood plasma with a further 20% (middle) or 50% (right) blood plasma solution present throughout the experiment (see Materials and Methods for protocol). Data points were acquired after 3 h and

indicate means from two independent experiments. Error bars denote upper and lower limits. NS indicates no significant difference for an ANOVA test with Tukey-Kramer post hoc analysis for pairwise comparisons.

Supplementary Table 1 | Strains and plasmids

Strain/plasmid	Genotype/description	References/ Sources
E. coli		
DH5α	Cloning strain, F´ *proA*$^{+}$*B*$^{+}$ *lacI*^{q} Δ*(lacZ)M15 zzf::Tn10* (Tet^{R}) */ fhuA2*Δ*(argF-lacZ)U169 phoA glnV44 Φ80Δ(lacZ)M15 gyrA96 recA1 relA1 endA1 thi-1 hsdR17*	NEB
S. aureus		
RN4220	Restriction-deficient mutant of strain 8325-4, transformable cloning host	[1]
RN9011	RN4220 containing pRN7023 (SaPI-1 integrase)	[2]
RN6390b	Standard *agr*-I wild-type, derivative of NTCT8325-4	[3]
RN6911	RN6390b replacing *agrBDCA* and *RNAIII* with *tetM* (Δ*agrBDCA* Δ*RNAIII*)	[4]
RN6607	Standard *agr*-II wild-type	[6]
MK231	RN6911 SaPI-1*attC*::pMK031 (*sarAP1- mturquoise2* in the genome)	This study
MK232	RN6911 SaPI-1*attC*::pMK032 (*sarAP1-gfpmut2* in the genome)	This study
MK233	RN6911 SaPI-1*attC*::pMK033 (*sarAP1-mko* in the genome)	This study
MK241	MK231 containing pMK051	This study
MK242	MK232 containing pMK051	This study
MK243	MK233 containing pMK051	This study
MK244	MK232 containing pMK014	This study
MK245	MK232 containing pMK004	This study
MK260	RN6911 SaPI-1*attC*::pMK060 (*agrP2-agrCA* in the genome)	This study

MK261	MK264 containing pMK004	This study
MK264	RN6911 SaPI-1*attC*::pMK064 (*agrP2-agrCA*, *agrP3-mkate2* in the genome)	This study
MK265	MK264 containing pMK012	This study
MK121	RN6390b containing pMK021; *agr*P3-*gfpmut2*, *sarA*P1-*mkate2* Note that pMK021 does not contain *agrP2-agrCA.*	[5]
MK131	Methicillin resistant strain (MRSA), clinical isolate from human skin, *agr* group I strain containing pMK021; *agr*P3-*gfpmut2*, *sarA*P1-*mkate2*	[5]
MK125	RN6390b containing pMK013; *sarAP1-mko*	This study
MK126	RN6607 containing pMK013; *sarAP1-mko*	This study
Plasmids		
pMK004	pCN54 (Erm^r) containing *agrP3-mkate2*	[5]
pMK011	pCN54 (Erm^r) containing *sarAP1-mturquoise2*	This study
pMK012	pCN54 (Erm^r) containing *sarAP1-gfpmut2*	This study
pMK013	pCN54 (Erm^r) containing *sarAP1-mko*	This study
pMK014	pCN54 (Erm^r) containing *sarAP1-mkate2*	[5]
pRN7062	pCN54 (Erm^r) containing *agrP2-agrCA*, *agrP3-lacZ*	[6]
pMK051	pCN54 (Erm^r) containing *agrP2-agrCA*, *agrP3-mkate2*	This study
pJC1111	SaPI-1 *attS* suicide vector containing cadmium resistant (*cadCA*)	[7]
pMK031	pJC1111 (Cad^r) containing *sarAP1-mturquoise2*	This study
pMK032	pJC1111 (Cad^r) containing *sarAP1-gfpmut2*	This study
pMK033	pJC1111 (Cad^r) containing *sarAP1-mko*	This study
pMK060	pJC1111 (Cad^r) containing *agrP2-agrCA*	This study

pMK064	pJC1111 (Cad^r) containing *agrP2-agrCA, agrP3-mkate2*	This study

Supplementary Table 2 | Oligonucleotide primers.

Primers	Sequence (5'-3')
MKF011	TCGTTAACTAATTAATTTAAGAAGGAGATATACATATGGTATCAAAAGGGGAAGAGTTG
MKR011	TTAGAATAGGCGCGCCTTATTTGTACAGTTCGTCCATGCC
MKF013	TCGTTAACTAATTAATTTAAGAAGGAGATATACATATGAGTAAAGGAGAAGAACTTTTCACT
MKR013	TTAGAATAGGCGCGCCTTATTATTTGTATAGTTCATCCATGCCATG
MKF014	TCGTTAACTAATTAATTTAAGAAGGAGATATACATATGGTGAGTGTGATTAAACCAGAG
MKR014	TTAGAATAGGCGCGCCTTAGGAATGAGCTACTGCATCTTCTA
MKF031	TATAATAGCATGCACATAACACCAAAAAGAAGAAGGTGC
MKR031	CCGCAAAGGCGCCTGTCACTTTGCTTGATATATGAG
MKF032	AATACGCCGTTAACTGACTTTATTATCTTATTATATTTTTTTAACGTTTCTCACCGATGC
MKR032	GGAGGGGCTCACGACCATACTTACATGTCAACGATAATACAAAATATAATACAAAATATA
MKF033	TTGAATACGCCGTTAACTGACTTTATTATCTTATTATATTTTTTTAACGTTTCTCACCGA
MKR033	GGAGGGGCTCACGACCATACTTA

Supplemental Video Legends:

Supplemental Video 1 | *S. aureus* Agr quorum sensing is activated by surface-attached AIP-I. Time series of merged fluorescence images of the *S. aureus* reporter strain in the presence of Surface-PEG_{10000}-triazole-AIP-I (top left), Surface-PEG_{10000}-triazole-AIP-I + 2.5 μM TrAIP-II in solution (top right), Surface-PEG_{10000}-azide (bottom left), and Surface-PEG_{10000}-triazole-Linear-AIP-I (bottom right). The time interval between each image is 30 min.

Supplemental Video 2 | *S. aureus* Agr quorum sensing is inhibited by surface-attached TrAIP-II. Time series of merged fluorescence images of the *S. aureus* reporter strain in the presence of Surface-PEG_{10000}-triazole-TrAIP-II + 30 nM AIP-I in solution (top left), Surface-PEG_{10000}-triazole-TrAIP-II + 1 μM AIP-I in solution (top right), Surface-PEG_{10000}-azide + 30 nM AIP-I in solution (bottom left), and Surface-PEG_{10000}-triazole-Linear-TrAIP-II + 30 nM AIP-I in solution (bottom right). The time interval between each image is 30 min.

Supplemental Video 3 | Wild-type *S. aureus* responds to surface-attached AIP-I and TrAIP-II. Time series of merged fluorescence images of wild-type *S. aureus* strain in the presence of Surface-PEG_{10000}-azide (top left), Surface-PEG_{10000}-triazole-AIP-I (top right), Surface-PEG_{10000}-triazole-TrAIP-II (bottom left), and Surface-PEG_{10000}-triazole-TrAIP-II + 1 μM AIP-I in solution (bottom right). The time interval between each image is 30 min.

Supplementary Note 1:

Single cell-level analyses of the data in Fig. S1a showed that the *S. aureus* reporter cells displayed heterogeneous quorum-sensing responses (also shown in the main text Fig. 1b (vi) and Fig. 1c (vi)). To identify the source of heterogeneity, we measured the fluorescent protein distributions in individual cells under different conditions. The reporter cells that we used throughout the main text harbored the Agr-activated *agrP3* promoter fused to *mkate2* (*agrP3-mkate2*) and carried plasmid-expressed *agrCA* encoding the AIP-I detection-response apparatus under its native promoter, *agrP2* (*agrP2-agrCA*). Addition of 100 nM AIP-I to this strain resulted in a broad, skewed quorum-sensing controlled mKate2 protein production profile (red) compared to the narrow distribution of the GFPmut2 protein produced from the constitutive *gfpmut2* reporter gene (green) (Fig. S1a). The coefficient of variation for the normalized quorum-sensing response was σ/μ = 0.69 (±0.03) (yellow histogram in Fig. S1a). The broad mKate2 protein distribution could stem from differences in plasmid copy number per cell, variations in transcription from *agrP3* and/or *agrP2*, variations in translation of the mKate2 protein and/or AgrC-I/AgrA, variations in *agrP2-agrCA*, *agrP3-mkate2* gene copy numbers due to plasmid expression, or from intrinsically noisy *S. aureus* quorum-sensing responses due to feedback. We examined each of these possibilities.

First, we tested whether heterogeneity arises from variation in mKate2 fluorescent protein translation or from plasmid copy number effects. To do this, we replaced the *agrP3* promoter driving *mkate2* with the constitutive *sarAP1* promoter on the plasmid (*sarAP1-mkate2*). The corresponding histogram depicting the normalized mKate2 fluorescence is narrower when *sarAP1*, rather than *agrP3*, is the promoter upstream of *mkate2* (σ/μ= 0.22 (±0.02), yellow histogram in Fig. S1b). This result makes two points: first, mKate2 fluorescent protein translation is not

responsible for the heterogeneity we observed. Second, the result in Fig. S1b suggests that fluorescent protein production from the constitutive *sarAP1* promoter is homogeneous, irrespective of whether the gene is located on a plasmid or on the genome. Thus, plasmid copy number effects do not cause heterogeneity in this reporter system.

Next, we tested whether heterogeneity arises from variation in copy numbers of genes encoding the quorum-sensing-detection/response apparatus (*agrP2-agrCA*) from the plasmid. For this test, we introduced the *agrP2-agrCA* genes onto the genome rather than having them expressed from a plasmid. The reporter gene, *agrP3-mkate2*, was expressed from the plasmid (Fig. S1c). Addition of 100 nM AIP-I to this strain resulted in less broad, less skewed quorum-sensing controlled mKate2 protein production (red) compared to that of Fig. S1a. We could not determine the value of σ/μ for the normalized fluorescence distribution from the strain used in Fig. S1c, because the strain did not possess the constitutively expressed fluorescent protein gene. In a separate experiment, we used wild-type *S. aureus* RN6930b that encodes *agrP2-agrCA* as well as the *agrBD* genes on the genome, which provides the strain the capacity to make endogenous AIP-I (Fig. S1d). This wild-type strain also harbors the constitutively expressed *sarAP1-mkate2* gene as well as the quorum-sensing-controlled reporter gene, *agrP3-gfpmut2* on the same plasmid (Fig. S1d). This strain exhibited normalized fluorescence with σ/μ = 0.58 (±0.10), which is broader than that from the strain shown in Fig. S1b. We interpret these results to mean that expression of the *agrCA* genes from a plasmid that exists at about ~20 copies per cell[8] contributed to the observed heterogeneity but cannot be the sole source responsible for heterogeneity.

Lastly, we tested whether heterogeneity arises from variation in copy number of the *agrP3-mkate2* gene. For this assessment, we introduced both the *agrP3-mkate2* gene and the *agrP2-agrCA* gene onto the genome (Fig. S1e). This arrangement differs from the reporter strain shown

in Fig. S1a, which contains both *agrP2-agrCA* and *agrP3-mkate2* on the plasmid. Addition of 100 nM AIP-I to these cells resulted in a distribution with σ/μ = 0.20 (±0.04) that was narrower than that from the strains shown in Fig. S1a, S1c, and S1d. This result suggests that expression of the *agrP3-mkate2* gene from a multi-copy plasmid also partially contributed to the observed heterogeneity.

Taken together, these data indicate that heterogeneity from the reporter strain (Fig. S1a) is a consequence of expression of the *agrP3-mkate2* gene and the *agrP2-agrCA* gene when present on multi-copy plasmids. While we do not know whether the intrinsic properties of the Agr system (i.e., regulatory feedback) are responsible for the variation, one possibility is that the cells possess different numbers of AgrC-I receptors on their surfaces. AIP-I stimulation is known to induce a positive autoinduction feedback loop that promotes increased expression of *agrC*[9]. Initial differences in AgrC-I receptor numbers could be amplified through this feedback. This hypothesis is supported by our observation that the variation we measured positively depended on the concentration of AIP-I provided to the cells. Positive feedback could increase noise and make the *agrP3-mkate2* distribution broad, and such noise could be further amplified when there exist multiple copies of the *agrP3-mkate2* and the *agrP2-agrCA* genes when present on a plasmid (Fig. S1a). With respect to the present work, these analyses show that, while the plasmid-mediated *agrP3-mkate2* response to AIP-I is broad, it is a reliable and amplified readout of quorum sensing in the *S. aureus* reporter strain we have constructed (Fig. 1a).

We used the *S. aureus* reporter strain to follow the Agr quorum-sensing status for cells growing on non-modified and chemically-modified surfaces with confocal microscopy. Single-cell image analysis demonstrates that the *S. aureus* reporter cells exhibited a broad and skewed

quorum-sensing output growing on the Surface-PEG_{10000}-triazole-AIP-I with σ/μ = 0.67 (±0.03) (Fig. S5a), which is analogous to its response to native AIP-I in solution in Fig. S1a.

Supplementary Methods:

Solid phase peptide synthesis and peptide characterization. 2-chloro-trityl chloride resin was first derivatized with hydrazine monohydrate in dimethylformamide (DMF) for activation. Amino acids were coupled through standard Fmoc-based solid phase peptide synthesis. Note that the cysteine was protected with –StBu (or tert-butyl-thiolate). 4-pentynoic acid (5 equiv.) was activated by N,N'-diisopropyl carbodiimide (DIC, 20 equiv.) in 10 ml of CH_2Cl_2 under N_2 for 30 min before coupling to the peptide on resin for another 2 h[10]. The peptide was cleaved from the resin by stirring with a cleavage cocktail (95% TFA, 2.5% TIPS, and 2.5% H_2O) at room temperature for 2 h. The post-cleavage supernatant was precipitated with cold ether. The resulting pellet was washed twice with cold ether, dried under N_2 and purified by preparative reverse-phased high performance liquid chromatography (RP-HPLC) on a C18 column.

The cleaved and purified hydrazide peptide was subjected to oxidation and thioester formation at the C-terminus[11]. In the oxidation step, the peptide was dissolved in degassed oxidation buffer (6M guanidine hydrochloride and 100 mM phosphate at pH = 3) to a final concentration of 5 mM before reaction with 20 equiv. $NaNO_2$ for 20-30 min in a -10°C ice-salt water bath. Next, the system was brought back to room temperature and mixed with 100 mM MESNa dissolved in thiol buffer (6M guanidine hydrochloride and 100 mM phosphate) for in situ thioesterification. The pH was adjusted to 6. After running for 2 h, the reaction products were purified by semi-preparative RP-HPLC. The thioester precursor was lyophilized and redissolved

in cyclization buffer (50 mM TCEP, 100 mM phosphate of pH 7, 25% ACN) for cysteine deprotection and thiolactone formation[12]. The reaction was allowed to run for 2 h at room temperature, followed by purification through semi-preparative RP-HPLC and characterization through analytical RP-HPLC and ESI-MS (Fig. S3).

For generation of PEG_{330}-triazole-AIP-I and PEG_{330}-triazole-TrAIP-II, we performed the CuAAC click reaction to incorporate the O-(2-azidoethyl)heptaethylene glycol onto the Alkyne-AIP derivatives. The alkyne-AIPs and PEG_{330}-azide were brought to solution in 100 mM phosphate buffer at pH 7 at 200 μM and 400 μM, respectively. Copper catalyst and ligands were added at final concentrations of 0.10 mM $CuSO_4$ and 0.50 mM Tris(3-hydroxypropyltriazolylmethyl)amine, and subsequently treated with 5 mM sodium ascorbate. The reaction was mixed well and carried out for 1 h. At the end of the reaction, the system was quenched with 2 mM EDTA before purification by semi-prep RP-HPLC and characterization through analytical RP-HPLC and ESI-MS.

Quantification of peptide concentration. All Alkyne-AIPs and PEG_{330}-triazole-AIPs were quantified by ^{1}H-NMR[13]. This is a simple approach to determine sample concentration using a standard capillary and an external calibration sample of known concentration. First, 150 μM of DSS was dissolved in D_2O as the reference material for the standard capillary. Next, 3 mM glycine dissolved in D_2O was used as the calibration sample. Finally, we prepared the peptide samples in deuterated DMSO (DMSO-d6).

All ^{1}H NMR were performed on a 500 MHz NMR. The NMR spectrum of the glycine calibration sample containing the DSS standard capillary was acquired first, followed by that of

the peptide sample containing the same capillary. The intensities of the peaks of interest and of the reference capillary in the samples were determined through MNova (MestreLab) data processing software. In this study, peaks in the corresponding to aromatic protons (from Tyr in AIP-I and Phe in TrAIP-II) were integrated.

The concentration of any sample of interest is determined using equation [1]: *I* is the integral (or sum of integrals) of the peak(s) of interest, *#P* is the number of protons that contribute to the peaks of interest per molecule, and *C* is the overall concentration of the material in solution. The calibration material is glycine, where the peak of interest corresponds to the two protons at the alpha position. The capillary material is DSS with the peak of interest arising from the nine silicon-shielded methyl protons.

$$C_{sample} = C_{calibration\ material} \times \frac{\#P_{calibration\ material}}{\#P_{sample}} = \frac{\frac{I_{sample}}{I_{capillary\ in\ sample}}}{\frac{I_{calibration\ material}}{I_{capillary\ in\ calibration\ material}}} \qquad \textbf{[1]}$$

The derivation of equation [1] rests on the assumptions that each individual proton in the sample contributes the same amount of area to the peak integral, and that $\#P_{capillary} \times C_{capillary}$ is constant for both the calibration sample and the sample of interest because the same capillary insert is used for the two samples.

Supplementary References:

1 Kreiswirth, B. N. *et al.* The toxic shock syndrome exotoxin structural gene is not detectably transmitted by a prophage. *Nature* **305**, 709-712 (1983).

2 Ruzin, A., Lindsay, J. & Novick, R. P. Molecular genetics of SaPl1 - a mobile pathogenicity island in *Staphylococcus aureus*. *Mol Microbiol* **41**, 365-377 (2001).

3 Novick, R. P. Genetic Systems in Staphylococci. *Method Enzymol* **204**, 587-636 (1991).

4 Novick, R. P. *et al.* Synthesis of staphylococcal virulence factors is controlled by a regulatory RNA molecule. *Embo J* **12**, 3967-3975 (1993).

5 Kim, M. K., Ingremeau, F. B., Zhao, A., Bassler, B. L. & Stone, H. A. Local and global consequences of flow on bacterial quorum sensing. *Nature Microbiology* **1**, 15005 (2016).

6 Lyon, G. J., Mayville, P., Muir, T. W. & Novick, R. P. Rational design of a global inhibitor of the virulence response in *Staphylococcus aureus*, based in part on localization of the site of inhibition to the receptor-histidine kinase, AgrC. *P Natl Acad Sci USA* **97**, 13330-13335 (2000).

7 Geisinger, E., George, E. A., Muir, T. W. & Novick, R. P. Identification of ligand specificity determinants in AgrC, the *Staphylococcus aureus* quorum-sensing receptor. *J Biol Chem* **283**, 8930-8938 (2008).

8 Charpentier, E. *et al.* Novel cassette-based shuttle vector system for gram-positive bacteria. *Appl Environ Microb* **70**, 6076-6085 (2004).

9 Novick, R. P. & Geisinger, E. Quorum sensing in Staphylococci. *Annu Rev Genet* **42**, 541-564 (2008).

10 Lu, J., Shi, M. & Shoichet, M. S. Click chemistry functionalized polymeric nanoparticles target corneal epithelial cells through RGD-cell surface receptors. *Bioconjugate Chem* **20**, 87-94 (2009).

11 Zheng, J. S., Tang, S., Qi, Y. K., Wang, Z. P. & Liu, L. Chemical synthesis of proteins using peptide hydrazides as thioester surrogates. *Nat Protoc* **8**, 2483-2495 (2013).

12 George, E. A., Novick, R. P. & Muir, T. W. Cyclic peptide inhibitors of staphylococcal virulence prepared by Fmoc-based thiolactone peptide synthesis. *J Am Chem Soc* **130**, 4914-4924 (2008).

13 Fardink, J. R. Dr. Bence: A simple method for determining absolute concentration by ^{1}H NMR. *Department of Chemistry, Princeton University* (2010). Link: http://arks.princeton.edu/ark:/88435/dsp01m039k5538

Color-blind-friendly versions of Figures 1-5 and Supplementary Figures 1-8:

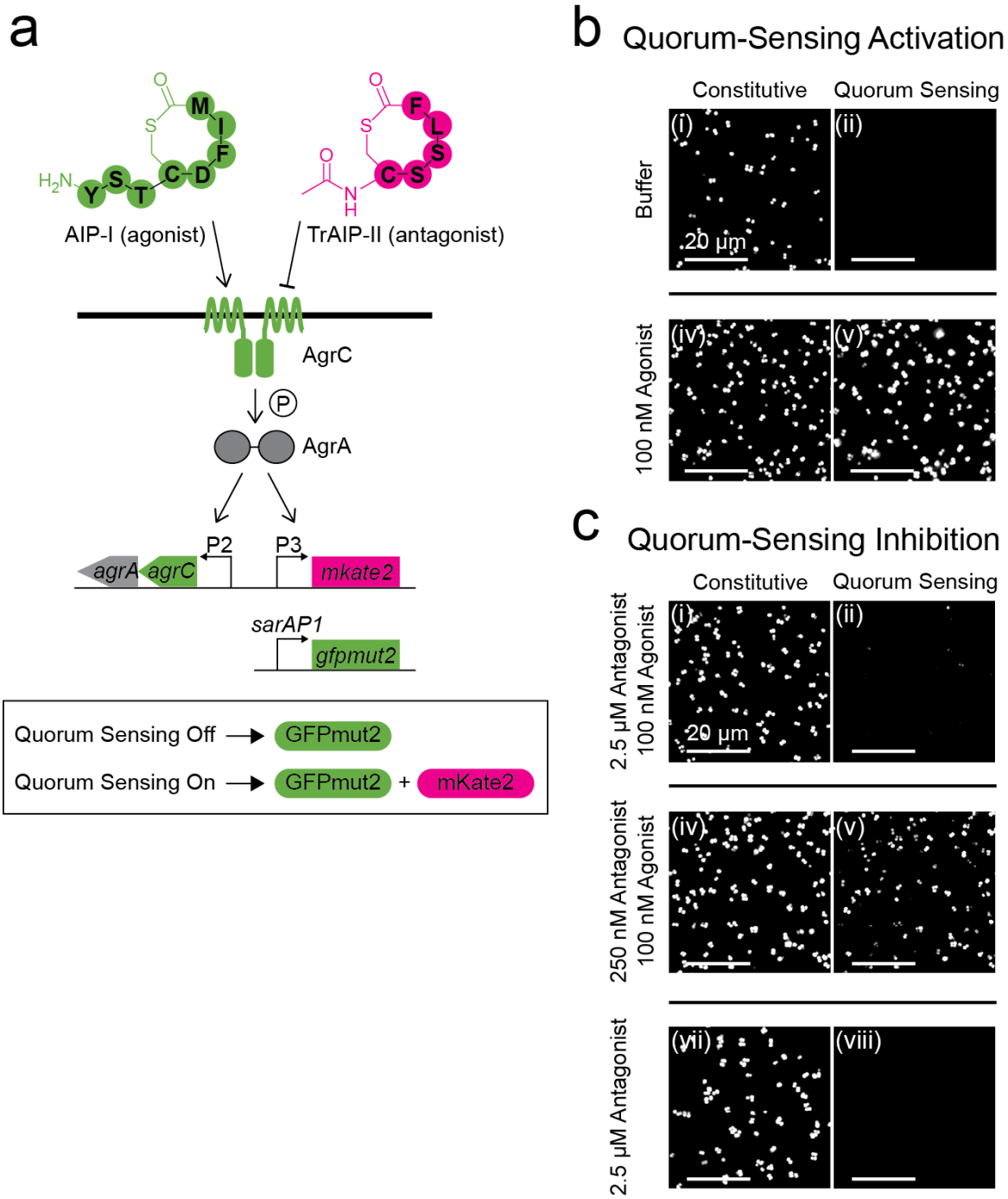

Figure 1 | A strategy to quantify the Agr quorum-sensing responses of *S. aureus* to exogenously supplied agonists and antagonists.

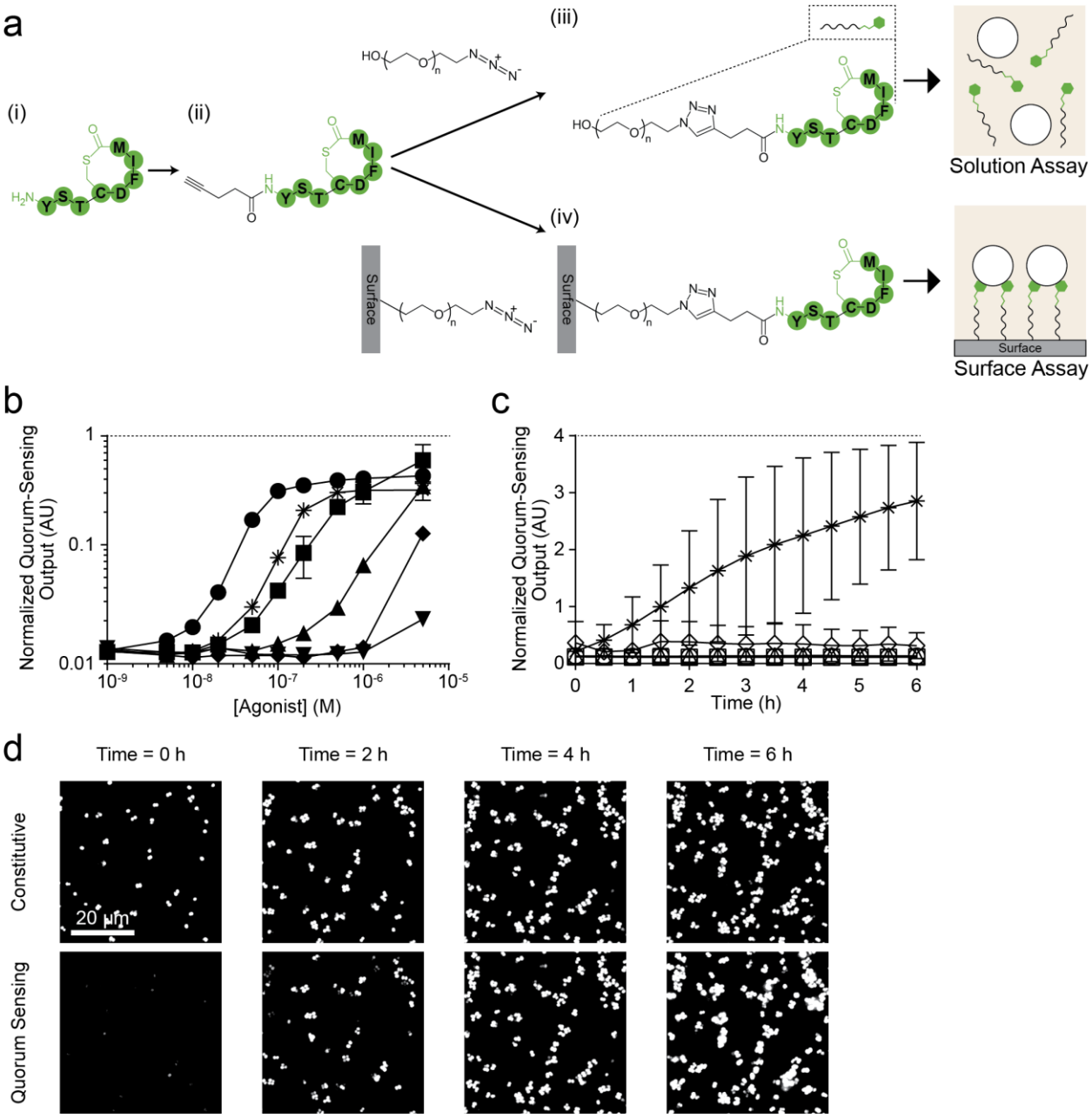

Figure 2 | *S. aureus* Agr quorum sensing is activated by surface-attached AIP-I.

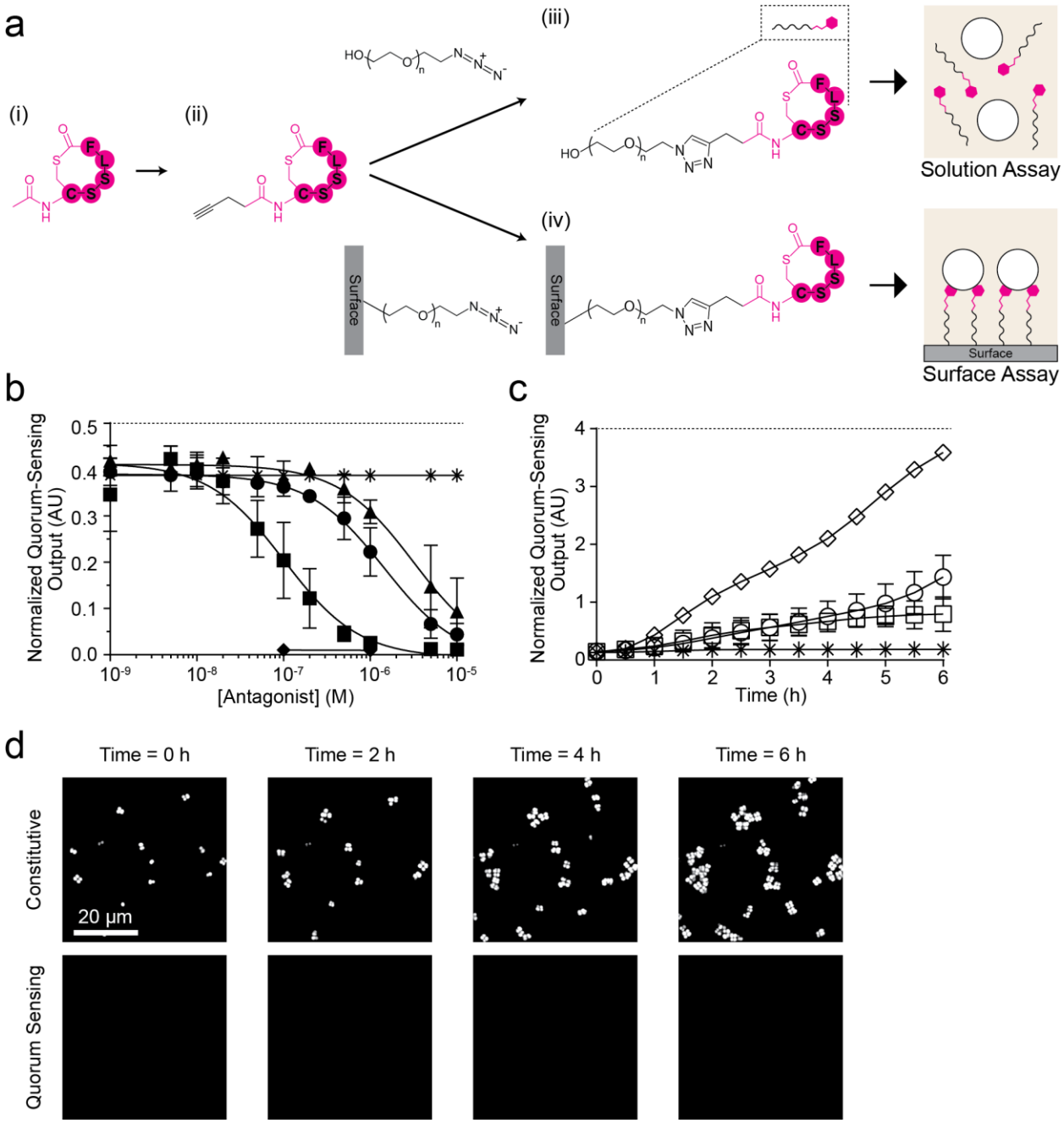

Figure 3 | A surface-attached Agr quorum-sensing antagonist, TrAIP-II, inhibits the *S. aureus* quorum-sensing response to AIP-I.

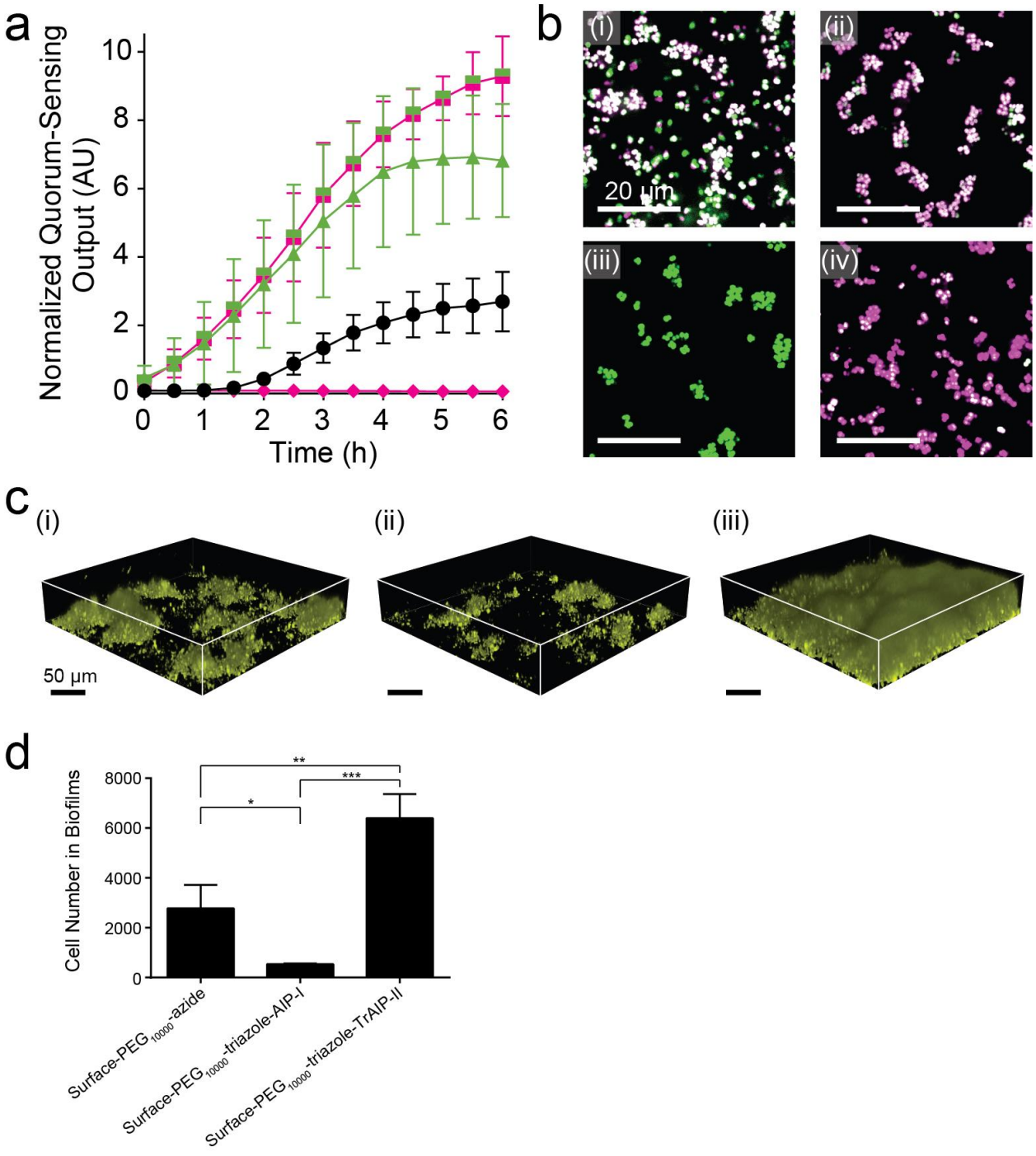

Figure 4 | Wild-type *S. aureus* responds to surface-attached AIP-I and TrAIP-II.

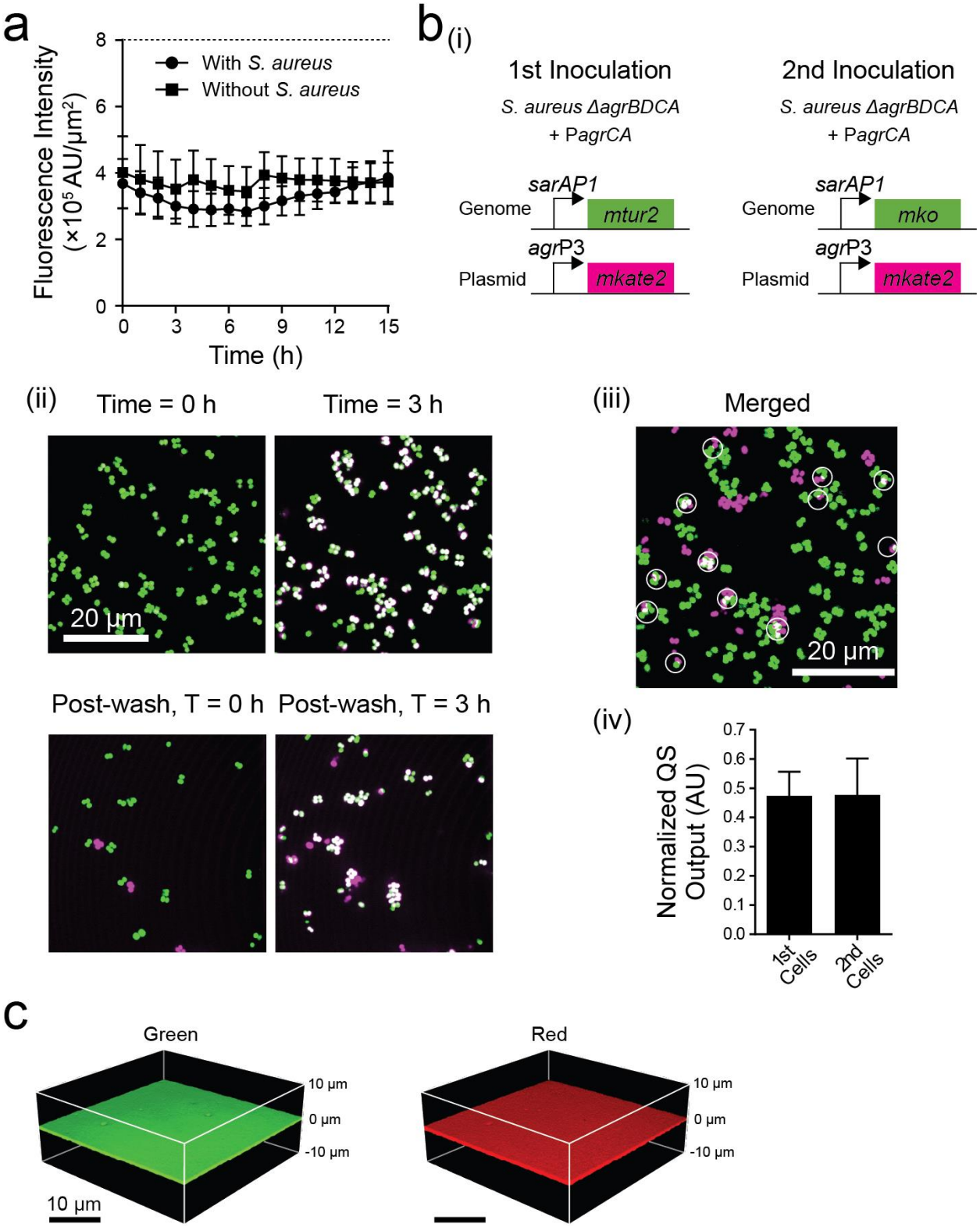

Figure 5 | Features of autoinducer-attached surfaces.

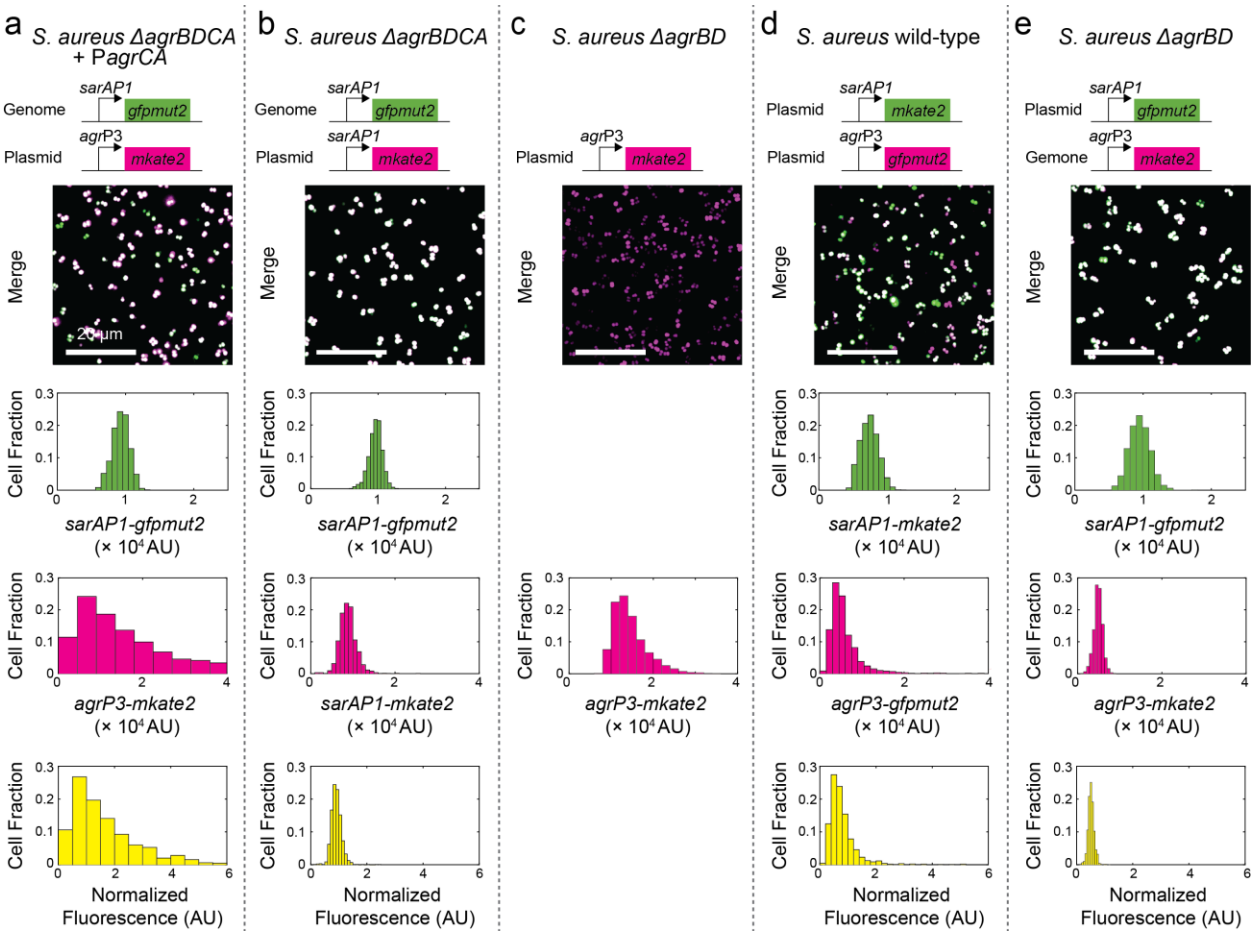

Supplementary Figure 1 | *S. aureus* exhibits heterogeneous quorum-sensing responses.

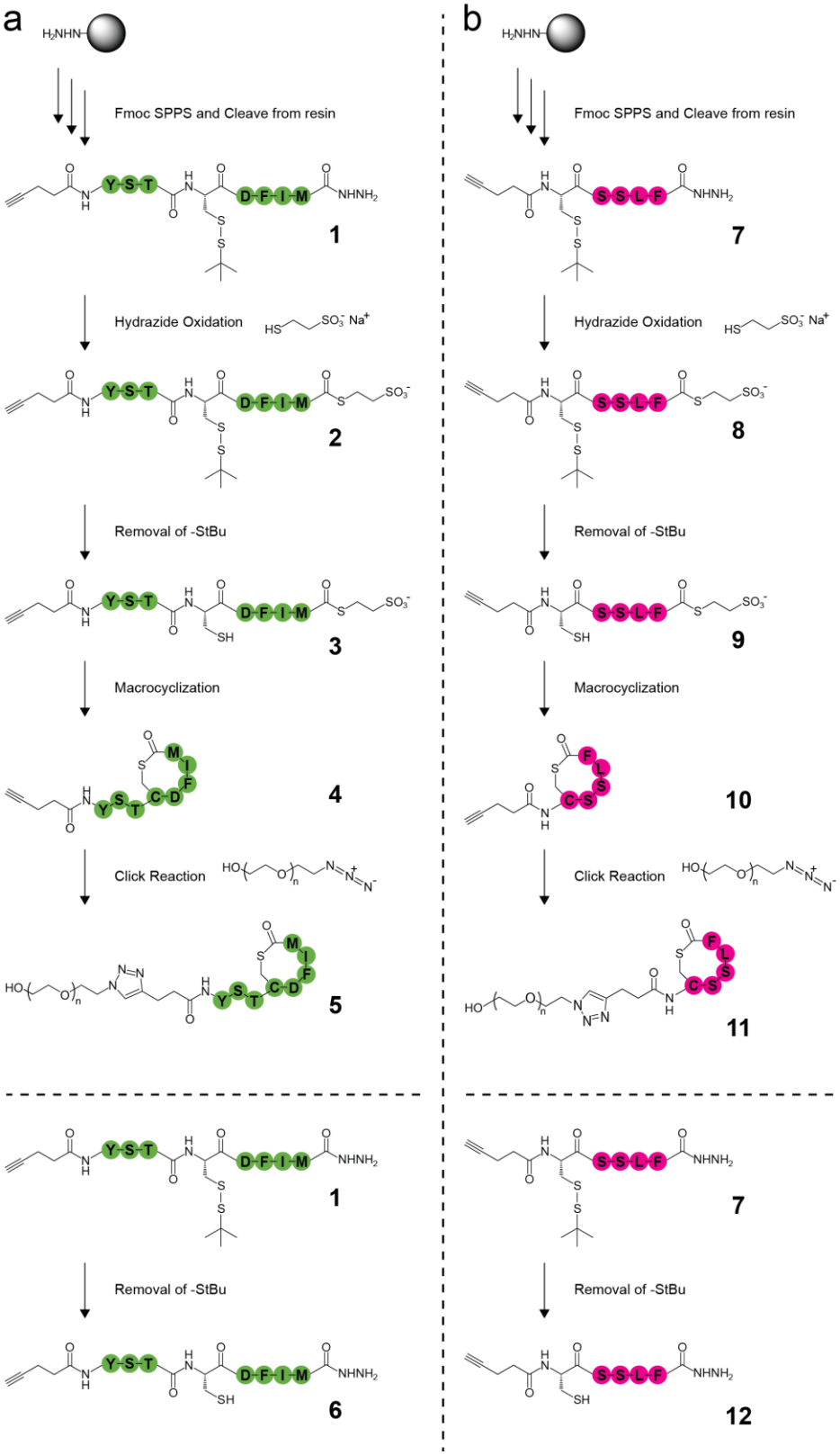

Supplementary Figure 2 | Synthesis scheme for a, AIP-I derivatives and b, TrAIP-II derivatives.

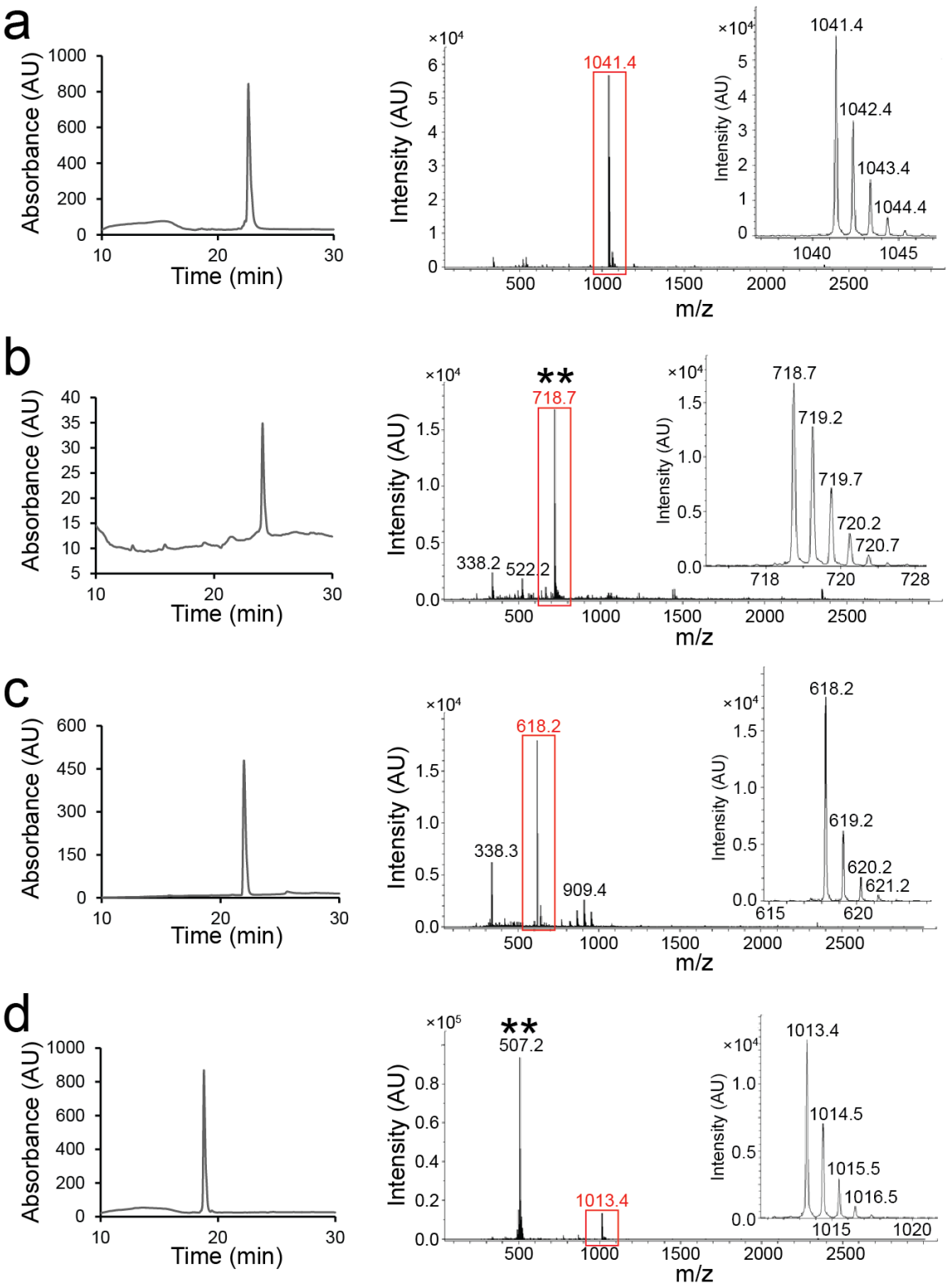

Supplementary Figure 3 | Characterization of purified AIP-I and TrAIP-II derivatives by RP-HPLC (left) and electrospray ionization-mass spectrometry (ESI-MS, right).

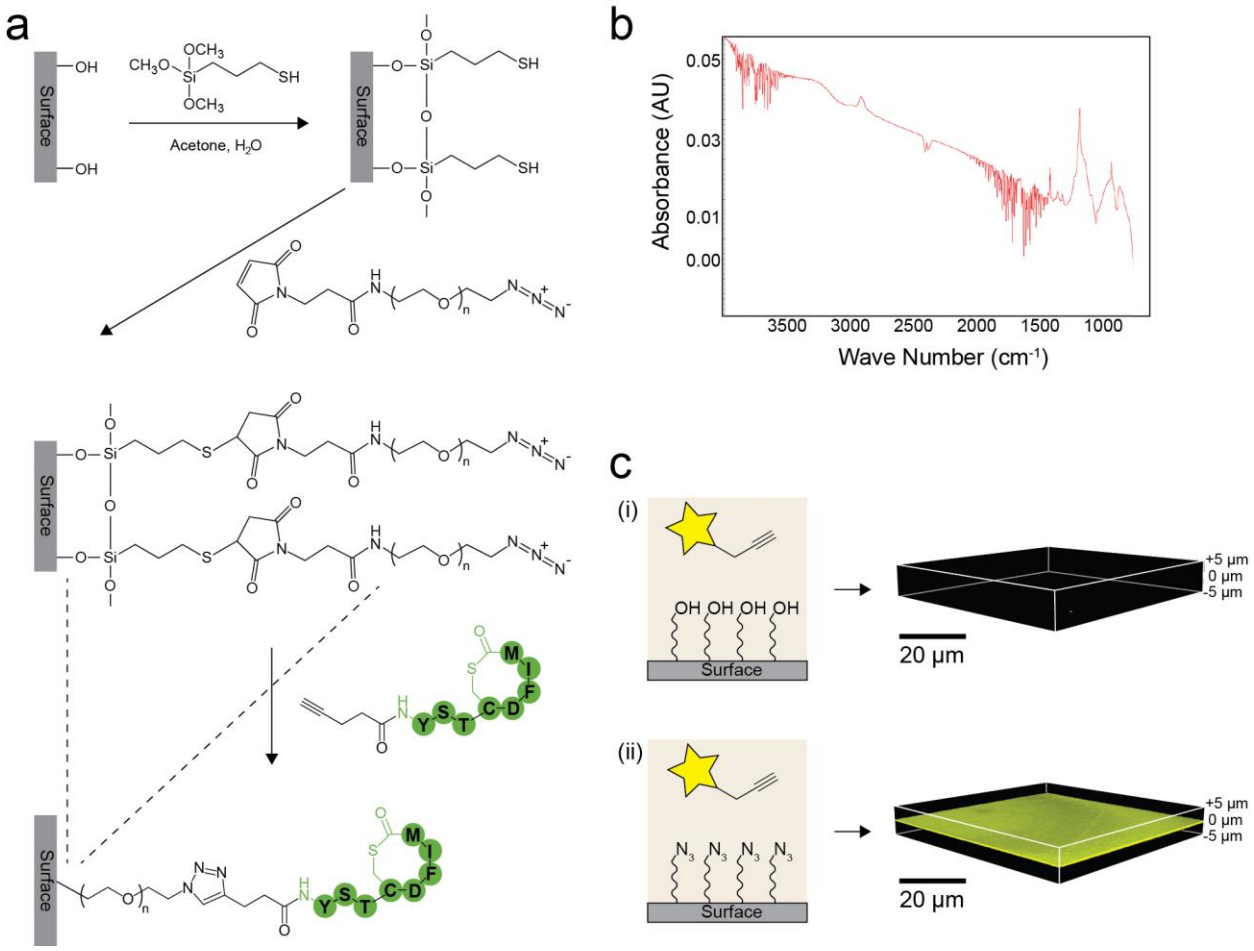

Supplementary Figure 4 | Chemical modifications of surfaces and surface chemistry characterization.

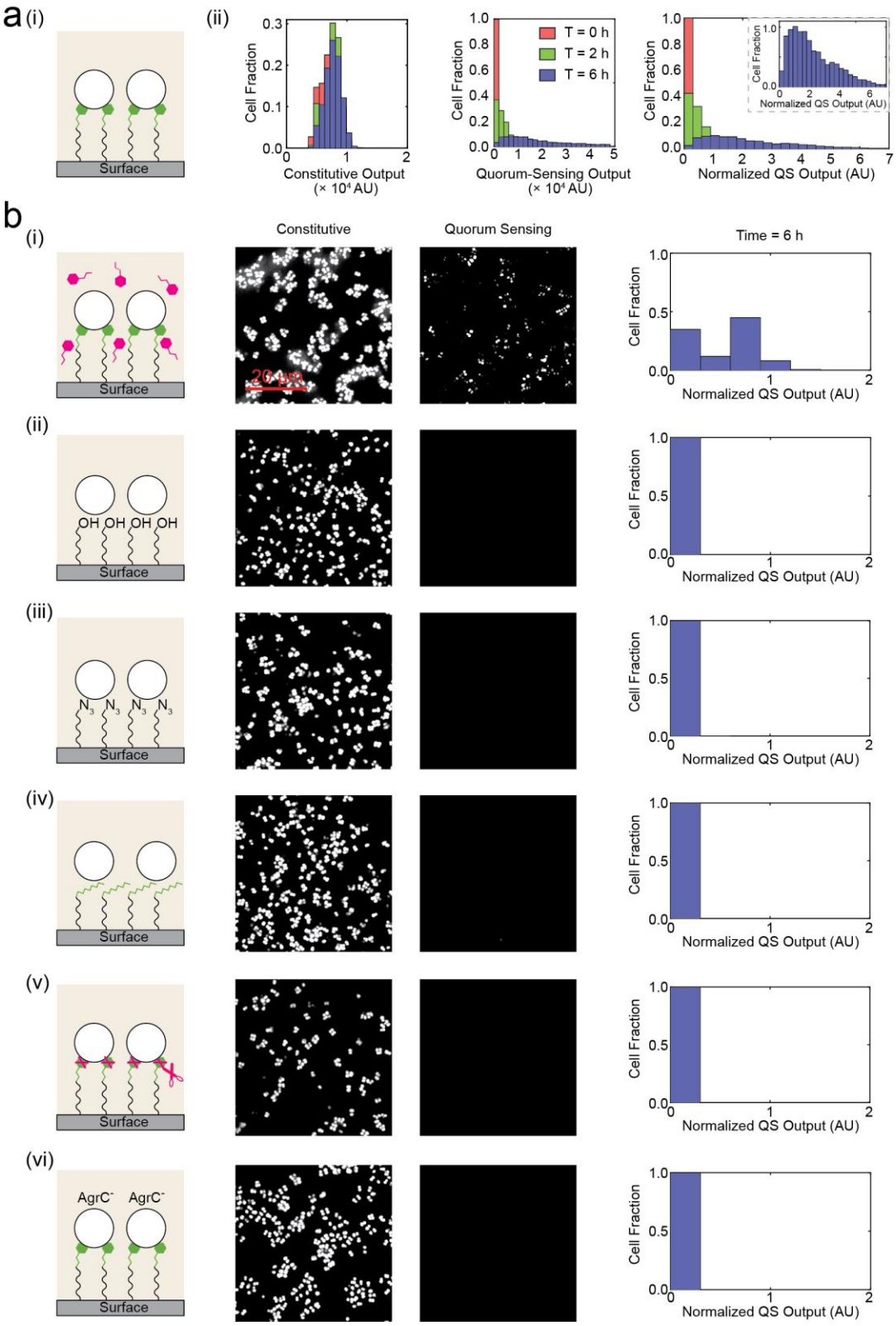

Supplementary Figure 5 | *S. aureus* Agr quorum sensing is activated by surface-attached AIP-I.

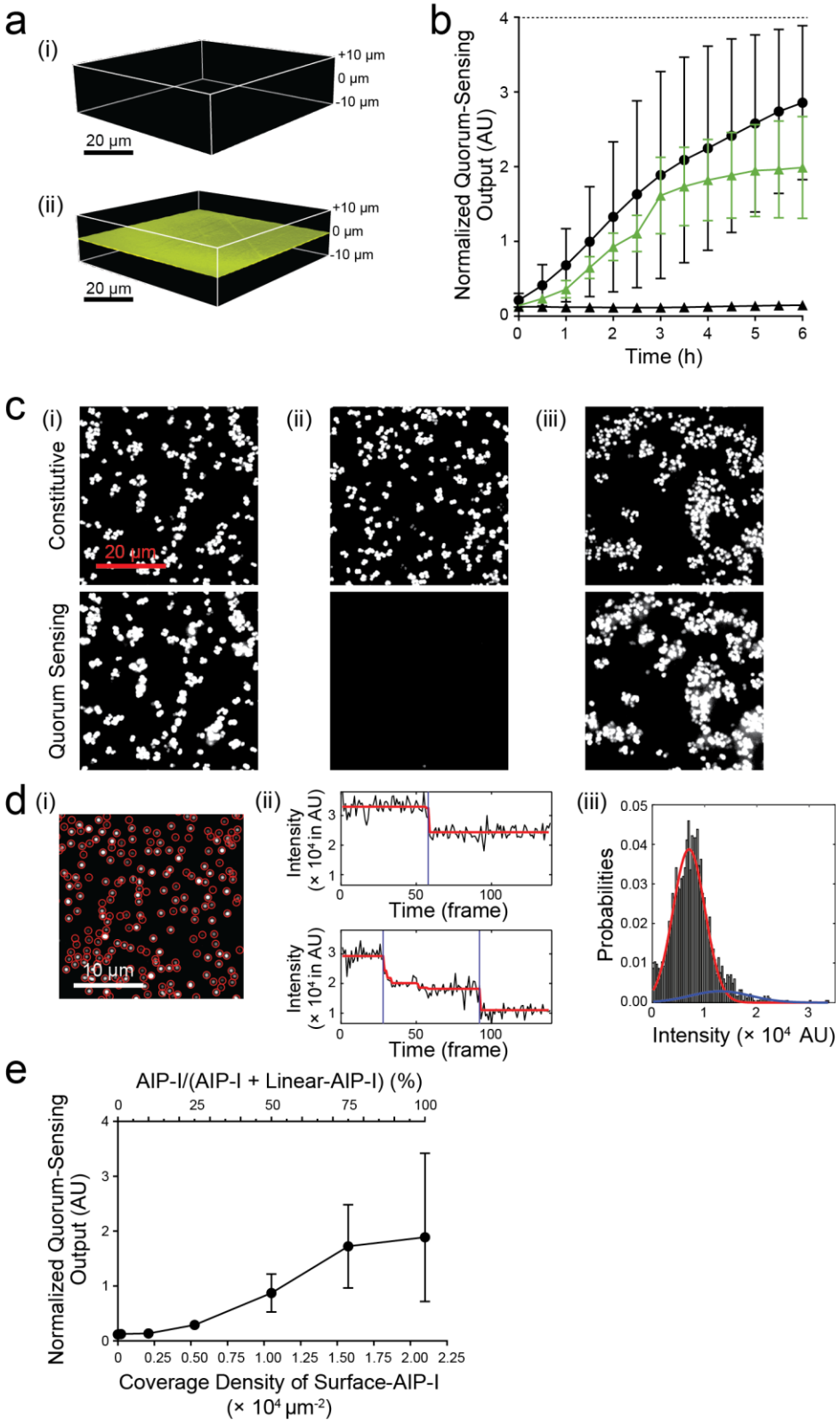

Supplementary Figure 6 | The requirements for Agr quorum-sensing activation by surface-attached AIP-I.

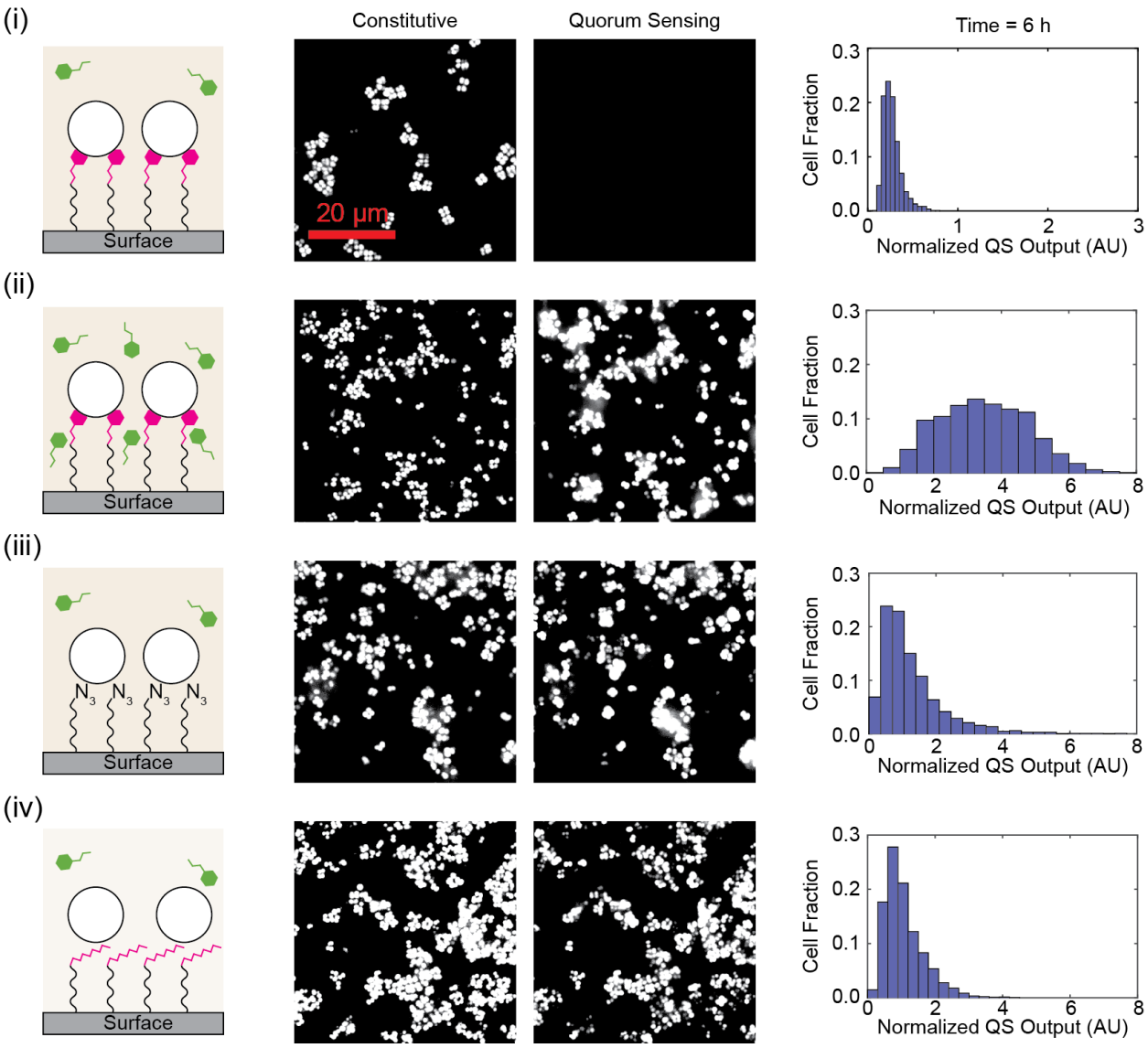

Supplementary Figure 7 | *S. aureus* Agr quorum sensing is inhibited by surface-attached TrAIP-II.

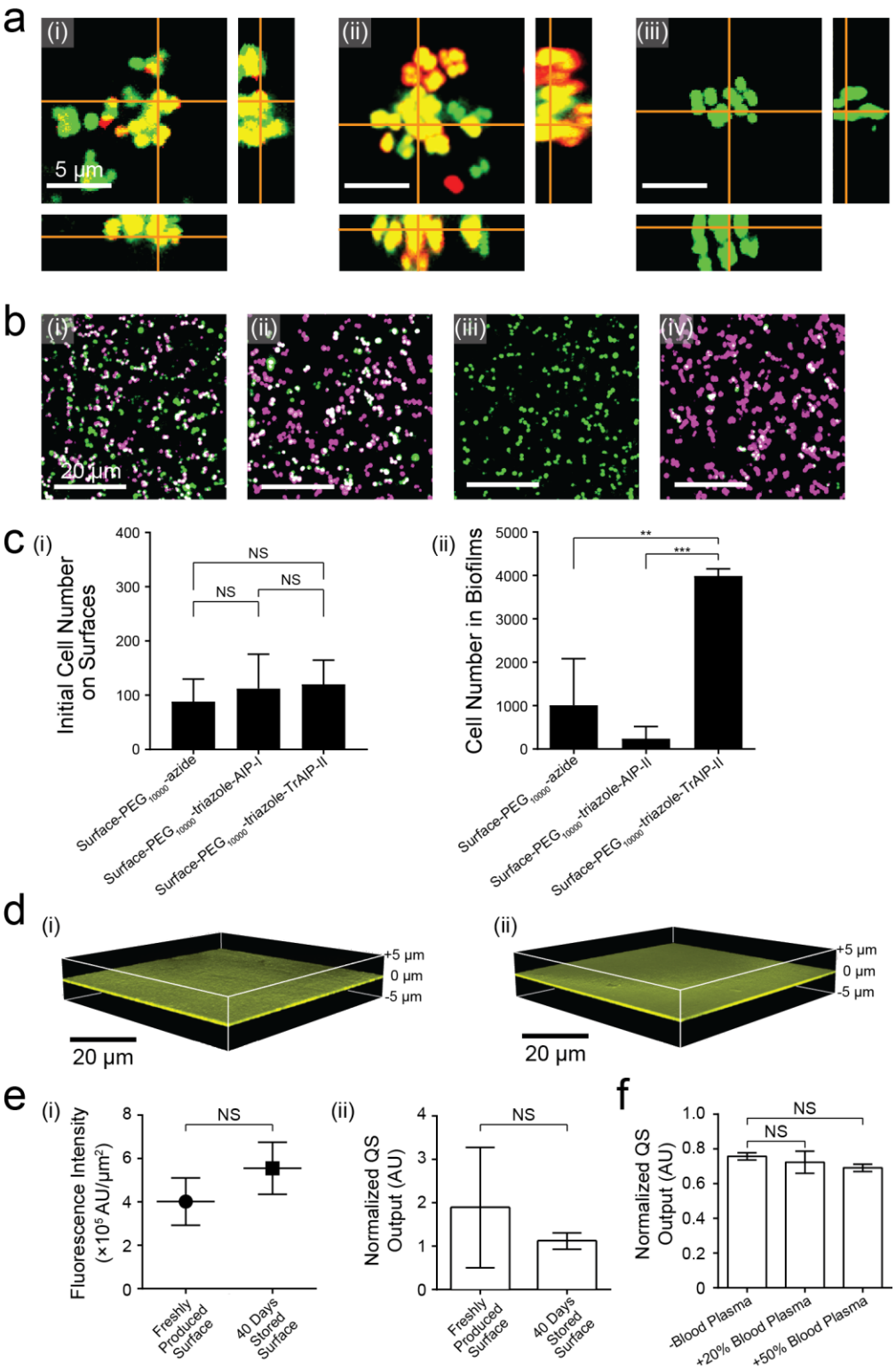

Supplementary Figure 8 | Quorum-sensing response of wild-type *S. aureus* to surface-attached AIP-I, AIP-II, and TrAIP-II, chemical modification of metal and plastic surfaces, and examination of stability of the chemically-modified surfaces.